Master Thesis:
Power ramp rate reduction in photovoltaic power plants using energy storage

Group:PED4-1045

Department of Energy Technology

Dimitar Nikolov Nikolov

DEPARTMENT OF ENERGY TECHNOLOGY
AALBORG UNIVERSITY

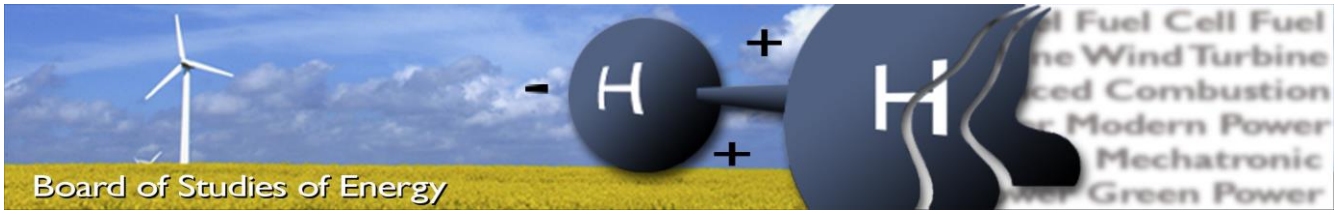

Title: Power ramp rate reduction in photovoltaic power plants using energy storage
Semester: 4th Semester Master Thesis
Semester theme: Master Thesis
Project period: 6.02.2017-01.06.2017
ECTS: 30
Supervisor: Dezso Sera and Sergiu Spataru
Project group: PED4-1045

Dimitar Nikolov Nikolov

SYNOPSIS:

The share of energy supplied by renewable energy is expanding every year. The renewable energy sources, like wind and solar, have a variable power profile.

This project focuses on the strategies to lessen the uneven supply of power provided by photovoltaic generators, due to cloud shadows, with the help of an energy storage system.

Two low pass filters and one gradient based method are investigate in detail. Simulations with different irradiance profiles are performed, to evaluate the methods weaknesses and strengths. Parameters, like battery size, smoothing performance, battery utilization, etc. are discussed. At the end the approaches are implemented experimentally, and their effectiveness appraised.

Keywords: power smoothing, battery, ramp rate, PV generator, energy storage,

Pages, total: [-]
Appendix: [-]
Supplements: [-]

By accepting the request from the fellow student who uploads the study group's project report in Digital Exam System, you confirm that all group members have participated in the project work, and thereby all members are collectively liable for the contents of the report. Furthermore, all group members confirm that the report does not include plagiarism.

DEPARTMENT OF ENERGY TECHNOLOGY
AALBORG UNIVERSITY

Contents

Chapter 1 Introduction 4
A. Problem statement 5
B. Objectives 5
C. Project Limitations 6
Chapter 2 Overview of PV Power Smoothing Methods 7
A. Low Pass Filter Method 7
B. Moving Average Method 8
C. Exponential Moving Average 9
D. Ramp Rate Control Based on Gradient 9
E. Selection of methods 11
Chapter 3 Modeling of PV Generator, and Battery Energy Storage System 12
A. Modeling of PV Panels 12
B. Modeling of Li-ion Battery 14
Chapter 4 Evaluation of Smoothing Methods – Simulation 18
A. First Order Low Pass Filter Method 21
B. Ramp Rate Control Based on Gradient Method 23
C. Proposed Second Order Low Pass Filter Method 28
D. Comparison Between the Different Smoothing Methods and Battery Sizing 31
Chapter 5 Evaluation of Smoothing Methods – Experimental 37
A. First Order Low Pass Filter Method 38
B. Gradient Method 39
C. Second Order Low Pass Filter Method 41
Conclusions and future work 42
References 43

DEPARTMENT OF ENERGY TECHNOLOGY
AALBORG UNIVERSITY

Chapter 1 Introduction

Renewable energy sources have grown significantly in the last decades in a bid to reduce the impact of CO_2 emissions on the climate. However, wind and solar come with challenges such as short term output power variability. For solar power this is caused by the shadows cast by clouds, blocking part of the irradiance falling on the photovoltaic (PV) generator. These fluctuations in power can lead to voltage variations, and frequency offset, affecting grid stability [1].

The decrease in PV panel prices in recent years, has led to a growth in PV installations [2], both on industrial and residential levels. Consequently some grid operators have introduced limits for the ramp rate of power [3] that can be fed into the grid. Thus the control strategies to achieve smooth PV power output can be separated into two groups. The first one modifying the already existing control schemes of the system, for example by modifying the maximum power point tracking method in [4]. Second adding an additional element in the form of energy storage system to the PV generator. Multitude of energy storage systems(ESS) have been investigated in the literature, like the electric double-layer capacitors [5], fuel cell [6], and battery energy storage [7],[8]. The most obvious choice for residential applications of storage is rapidly coming to be batteries. The Li-ion batteries are particularly suitable, because they do not require maintenance once installed, and are experiencing a fall in prices, in part as a response to the commercialization of electric vehicles [9]. They have many upsides like the long lifetime, high efficiency, high energy density, etc. There are a few control schemes proposed in the literature to manage the generation, storage, and utilization of the produced energy for self-consumption and peak shaving [10],[11] . Additionally, there are papers focused on using the energy storage for purely power smoothing application, with the aim to reduce variation in the renewable energy produced, shown on Fig. 1.

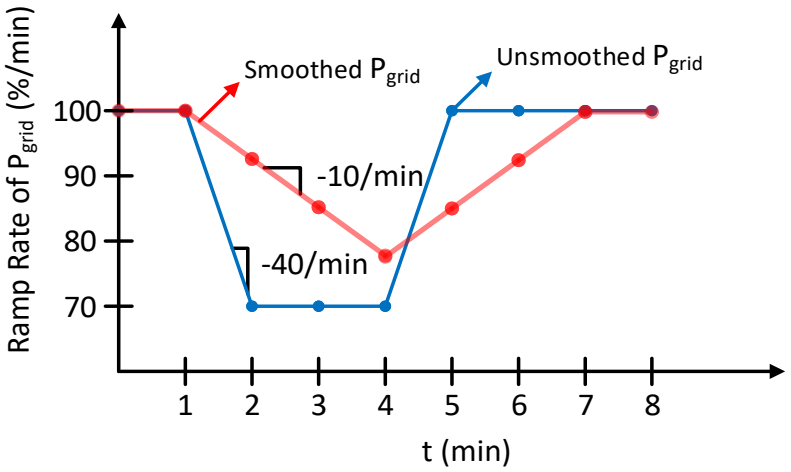

Fig. 1 Power smoothing with energy storage

The strategies for mitigating the power fluctuations of PV panels can be represented by the main approach to acquiring a smooth power reference. Firstly a first order low pass filter (LPF) [12],[13] can be used to mitigate the high frequency fluctuations. Second a moving average [7],[14] or an exponential moving average [6] approaches can be employed for a similar

result as the LPF. Finally a ramp rate control based on gradient involving the finding the gradient of the power reference [8], can be used. The use of LPF leads to a delay in the power reference, leading to unnecessary use of energy storage. Similar behavior is observed with the moving average methods, and their dependence on the past power values examined in [8] . However, the gradient method avoids this since it does not rely on past information.

A. Problem statement

The power produced by the photovoltaic generator varies, due to the change of external conditions like temperature, local weather, time of year, etc. The size of the PV system affects the power variability, in small residential PV generators the effect of shading, due to clouds, can result in steep power ramp rates, which are severely reduced in large scale plants [4], the attenuation is proportional with the square root of the PV plant area. As a result the produced power can have significant fluctuations. This may lead to voltage and frequency fluctuations, affecting the stability of weak grids.

With the increasing number of grids with PV generator this problem is becoming quite significant. Since the operators do not have control over the renewable generation, the control of the systems with PV and battery storage has to be optimized to achieve a smooth power delivery to the electrical network. There are requirements to limit the ramp rate of the power supplied to the network to 10 (%) of the rated power for the system per minute in Puerto Rico [15] and Germany[16] . The upward and downward fluctuations in power are can be managed by the grid operators to a curtain extend, however the rapid growth in renewable sources of energy, may lead to not enough available capacity in the grid to compensate the power fluctuations. Thus a control strategy has to be devised to mitigate the power fluctuations produced by the variability of the irradiation contacting the PV generator.

B. Objectives

The aim of this project is to investigate existing power smoothing strategies for PV power plants with energy storage. To limit the scope of this project the following power smoothing methods have been chosen from the literature:

- Low pass filter
- Moving average
- Exponential moving average
- Ramp rate control, based on slope

This project will focus on investigating the approaches which apply to a PV generator and an integrated battery storage system, with the aim of achieving the best possible ration between the power smoothing and the battery size. The two most promising power fluctuation mitigation approaches will then be selected. Tests will be performed both, in simulation, and experimental setup, to evaluate the best approach for power smoothing, and if any additional improvements can be added. Based on the results the minimum battery size for fulfilling ramp rate requirements using various smoothing methods will be estimated. The positive and negative aspects of the power smoothing methods will be presented, and a final conclusions in which the

approach that has the most advantages, i.e. small battery size, easy to implement, reliability, and robustness.

C. Project Limitations

Limitations encountered during the project:

- Only three days of irradiance data are considered in the project
- Simulation model in which the converters are considered to be ideal and are neglected
- Only the moving average, exponential moving average, first and second order LPFs, and the gradient method are considered
- The search time needed for the maximum power tracking in not considered

Chapter 2 Overview of PV Power Smoothing Methods

The general structure of a typical PV system with battery storage for power smoothing can be shown in Fig. 2, where the power smoothing block generates the reference power, which has to be followed by the energy storage used, in this case a battery. The PV array is connecter to a DC/DC boost converter with a maximum power tracking scheme. The battery is connected to the dc link by a bidirectional DC/DC converter. The battery is also connecter to the dc link by the DC/DC, and is used for used for smoothing, self-consumption, etc. The dc link is additionally connected to and inverter, which transforms it and feeds it into the grid. Before the methods are presented the way to calculate the ramp rate has to be discussed. According to [17],[18] the ramp rate can be calculated by finding the difference between the first and last point of any 60 second interval of power. Each of following methods to smooth the power presented below, replace the Power Smoothing block in Fig. 2 , while the rest of the system is identical.

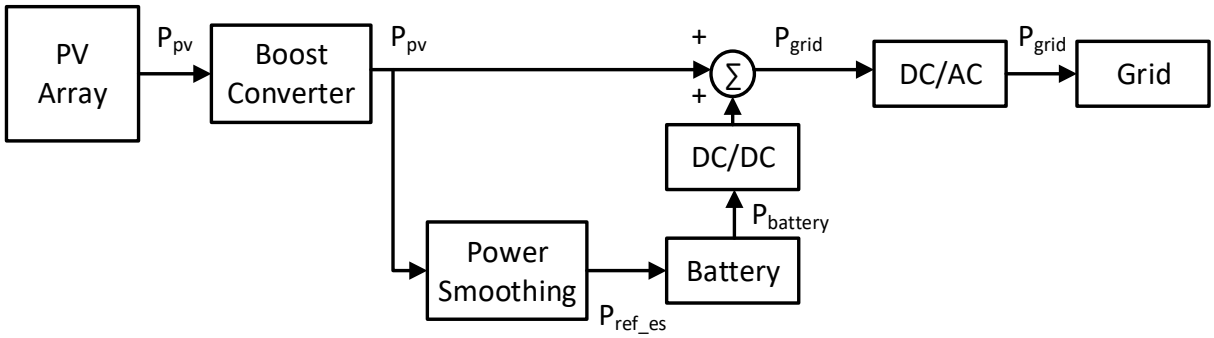

Fig. 2 General structure of PV with battery energy storage system

A. Low Pass Filter Method

Low pass filter is used to suppress the high frequencies, which reside over the cutoff frequency. The order of the filter determines how strict the bandwidth that passes signals is, the higher the order is the more abrupt is the reduction in the high frequency signals and the less of those signals are present in the filtered signal. The simplest implementation is a first order low pass filter proposed in [13], with a transfer function Eq.(2.1), where both the continuous and discrete forms are shown. The discrete form is derived using the Tustin approximation, where T_f the filter is time constant, and T represents the sampling period. The way to generate the power reference for the battery can be seen on Fig. 3.

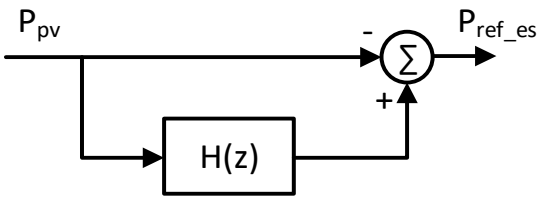

Fig. 3 Low pass filter implementation

To tune the filter solar irradiance for the high variation in irradiance day is used as a reference, where the grid ramp rate does not violate the 10 (%/min) of rated power for the PV panels. However, this cannot be guaranteed since a situation may arise when the PV power changes faster than the filter can smooth, leading to a violation in the ramp rate limit. If the time constant of the filter is too large, a larger battery will be needed, in the opposite case the battery maybe small, but the ramp rate of the power injected into the grid may exceed the imposed limit. A drawback of using a LPF is that during a clear sky day, with little variation in irradiance, the filter still generates a power reference, thus using the battery even when it is not needed. If a good analysis of the weather patterns is made, where the PV system is located, depending on the ratio between high irradiance variation days and clear sky days a compromise can be reached between partially fulfilling of the ramp limit and the least amount of battery capacity. It should be mentioned that the paper [13], does not propose a method to tune the filter as proposed here, they just suggest a 2 (min.) time constant.

$$H(s)=\frac{1}{\left(1+sT_f\right)}\rightarrow H(z)=\frac{z+1}{\left(1+\frac{2T_f}{T}\right)z+\left(1-\frac{2T_f}{T}\right)} \tag{2.1}$$

B. Moving Average Method

Moving average method presented in [7],[14] takes the past values of the PV power for a chosen period of time w, finding the average value for it Eq.(2.2), where n represents the current sampling value. Depending on whether the averaging period is large or small, the smoothing of the PV power will be more or less significant, respectively. Both paper proposes to use a 15 minute averaging interval to reduce power fluctuations. Similarly to the low pass filter method this approach cannot guarantee the fulfilling of the ramp rate limit, shown in [8]. The more aggressive the smoothing, the more battery power will be needed, since they are between adjacent peaks has to filled by the energy from the storage. Additionally, when the power fluctuations are small, like in a clear sky day, then the moving average method will still use the battery which is not desired. The implementation of the approach can be seen on Fig. 4.

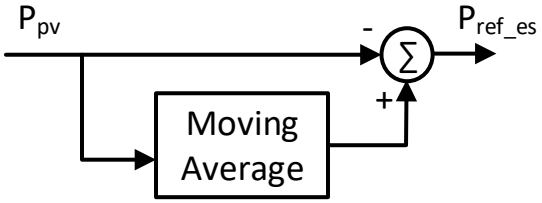

Fig. 4 Moving average implementation

$$P_{ref\_es}(n) = \frac{\sum_{i=0}^{w-1} P_{pv}(n-i)}{w} - P_{pv}(n) \tag{2.2}$$

C. Exponential Moving Average

The exponential moving average, proposed in [6], has a more complex form. It relies on the error of the previous prediction compared with the real value, which is then smoothed using a smoothing factor α and added to the previous prediction $P_{pv}(n-1)$. The method puts more weight on the last true value, compared with the simple moving average. The implementation can be seen on Fig. 5, and the formula to implement it is shown in Eq.(2.3). It has the same drawbacks as the moving average, and LPF approaches to power smoothing. Cannot guarantee that the ramp rate limit will not be exceeded, and results in usage of the energy storage when it is not needed, during a clear sky day.

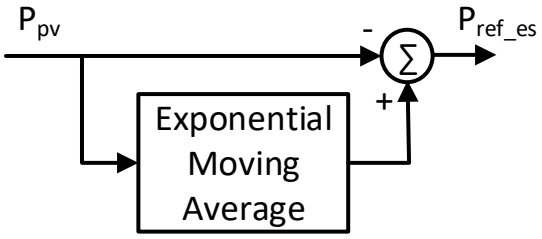

Fig. 5 Exponential moving average

$$P_{ref\_es}(n) = P_{pv}(n) - \alpha P_{pv}(n) + (1-\alpha)P_{pv}(n-1) \tag{2.3}$$

D. Ramp Rate Control Based on Gradient

The method proposed in [8] is based on a simplified version of the system in Fig. 2, presented in Fig. 6. Where the DC/DC converters are assumed to be ideal, thus their effect can be neglected. Additionally, the grid inverter is represented by its efficiency, which changes according to the power converter by the inverter, and can be implemented by a lookup table. This approach leads to Eq.(2.4), from which the reference gradient for the battery power can be derived Eq.(2.5). $\left.\frac{dP_{grid}}{dt}\right|_{des}$ represents the desired ramp rate that we want to follow, which is negative during a ramp down event, and positive during a ramp up event of the P_{pv}. It should be mentioned that the paper [8] does not specify what kind of value $\left.\frac{dP_{grid}}{dt}\right|_{des}$ should take during a constant P_{pv}.

$$\frac{dP_{grid}}{dt} = \eta_{inv}\left[\frac{dP_{pv}}{dt} + \frac{dP_{battery}}{dt}\right] \tag{2.4}$$

$$\frac{dP_{battery}}{dt} = \frac{1}{\eta_{inv}}\left[\left.\frac{dP_{grid}}{dt}\right|_{des} - \eta_{inv}\frac{dP_{pv}}{dt}\right] \tag{2.5}$$

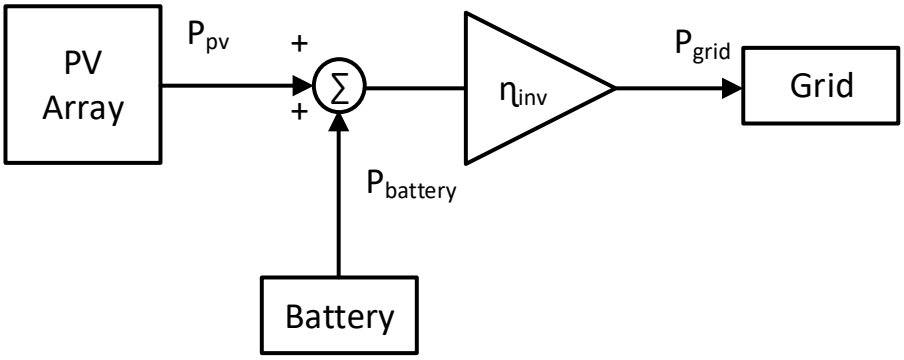

Fig. 6 Simplified system structure

The approach uses a dead zone, so the slow fluctuations of P_{pv} are not corrected when they are below the ramp rate limit shown on Eq.(2.6).

$$f\left(\frac{dP_{pv}}{dt}\right)=\begin{cases}0, & \text{if } \eta_{inv}\left[\frac{dP_{pv}}{dt}\right]\le\left.\frac{dP_{grid}}{dt}\right|_{des}\\ \frac{dP_{pv}}{dt}, & \text{otherwise.}\end{cases} \tag{2.6}$$

Additionally, a switch function is implemented to turn off the compensation, when the conditions presented in Eq.(2.7) are fulfilled.

$$S=\begin{cases}0, & \text{if } \left|P_{battery}\right|<\left.\frac{dP_{grid}}{dt}\right|_{des} \text{ and } f\left(\frac{dP_{pv}}{dt}\right)=0\\ 1, & \text{otherwise.}\end{cases} \tag{2.7}$$

Incorporating the conditions presented in Eq.(2.6) and Eq.(2.7) in Eq.(2.5). results in Eq.(2.8).

$$\frac{dP_{battery}}{dt}=S\frac{1}{\eta_{inv}}\left[\left.\frac{dP_{grid}}{dt}\right|_{des}-\eta_{inv}f\left(\frac{dP_{pv}}{dt}\right)\right] \tag{2.8}$$

To estimate the power reference for the battery $P_{battery}$ we can use Eq.(2.9), where $\frac{dP_{battery}}{dt}(n)$ is calculated using Eq. (2.8), T is the sampling period, and $P_{battery}(n-1)$ the value for the previous sampling period we calculated.

$$P_{battery}(n)=S\left[\frac{dP_{battery}}{dt}(n)T+P_{battery}(n-1)\right] \tag{2.9}$$

The method requires an energy storage system that can respond fast to changes in power. Additionally, this approach does not use previous values of the PV power like the LPF, and moving average methods presented before. During a clear sky day with slow variation of irradiance the ramp rate control based on gradient approach will not use the battery at all, as opposed to the previous three approaches. The implementation can be seen in Fig. 7, which incorporates the switch function to suppress the output, when the battery power is below the ramp rate limit and the gradient of the PV power is zero, forced by the dead zone function. It

should be mentioned that the paper proposes a droop loop to mitigate high gradient short duration variations in power. However this condition was not present in the requirements for limiting the ramp rate of a PV system, thus the droop loop was not implemented and is not presented in this report.

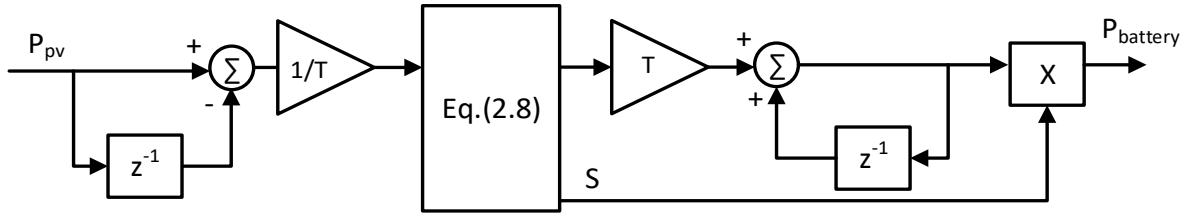

Fig. 7 Ramp Rate Base on Gradient implementation

E. Selection of methods

The LPF, moving average, and exponential moving average approaches, have similar drawback. They all are using the storage during a clear sky day, no irradiance fluctuations over 10(%) per minute, when ideally, we do not want any use of the battery. All three have to be tuned practically using data available for a highest variation in irradiance day, which does not guarantee fulfilling the ramp rate limit in event of more significant variation in the irradiance. However, they all are easy to implement and provide similar results. The biggest difference is in the computation power used, which is significantly larger for the Moving average and Exponential moving average methods, than the LPF approach.

Looking at the ramp rate approach, it is completely different to the other three ways to smooth the power. It is not active during a clear sky day and when the irradiance fluctuation is below the ramp rate limit. Additionally, it guaranties that the limit will not be violated, assuming battery is big enough to supply the needed power for smoothing. By changing the desired ramp rate, we can easily adapt it to different retirements for different systems, which is not the case for the previous methods.

Based on the above presented arguments the LPF, and the ramp rate based on gradient are selected to be implemented, both in simulation and practically. Additionally, a second order low pass filter will also be implemented, since it is not tested in literature, does not require high computational effort, and can be implemented in a straightforward way. It will be interesting to compare what effect doubling the steepness of the gain has on the filtered signal. However, it is tuned with the same methodology as the first order LPF. The continuous transfer function can be seen on Eq.(2.10), and using the Tustin approximation the discrete form ca be derived Eq.(2.11).

$$H(s) = \frac{w_n^2}{\left(s^2 + 2\zeta w_n s + w_n^2\right)} \tag{2.10}$$

$$H(z) = \frac{T^2 w_n^2 z^2 + 2T^2 w_n^2 z + T^2 w_n^2}{\left(T^2 w_n^2 + 4T\zeta w_n + 4\right) z^2 + \left(2T^2 w_n^2 - 8\right) z + \left(T^2 w_n^2 - 4T\zeta w_n + 4\right)} \tag{2.11}$$

Chapter 3 Modeling of PV Generator, and Battery Energy Storage System

The model of PV system with battery storage presented in Fig. 2, incorporates all the needed components to practically implement the setup. The ramp rate of grid power is calculated in the time span of minutes, while the dynamics in the converters take place in millisecond to microsecond range. Since we are investigating the dynamics of the system taking place in the scale of minutes to hours, the dynamics taking place in the converters, will have negligible effect on the power produced. This allows us to reduce the complexity of the system by removing the converters from Fig. 2, and working directly with the PV, battery, and grid power. This compromise is needed, since the additional complexity introduced by the converters, and grid in the simulation demands a quite high amount of computational power, and active memory. Although the removal of the converters will lead to high efficiency in simulation compared with the experimental setup, the gradients of the upward and downward ramp rate events of photovoltaic power, should not be affected.

A. Modeling of PV Panels

To simulate the behavior of the PV array, the Sandia photovoltaic array performance model described in [19] is used. The model is primarily suited for the flat-plate modules, concentrated modules, and large array of modules. The Sandia model is empirically derived, and its equations are obtained from individual solar cells characteristics, which leads to its high accuracy and versatility. All electrical, thermal, solar spectral, and optical effects are accounted for, and the model has been extensively tested in practice.

The electrical performance of the PV system is modeled using the following Eq.(3.1) estimates the short circuit current I_{sc}, Eq. (3.2) the current at maximum power point I_{mp}, Eq.(3.3) the open circuit voltage V_{oc}, Eq.(3.4) the voltage at maximum power V_{mp}, Eq. (3.5) the maximum power P_{mp}, and Eq. (3.6) the fill factor FF.

$$I_{sc} = I_{sco} f_1(AM_a)\left[\frac{E_b f_2(AOI) + f_d E_{diff}}{E_o}\right]\left[1+\alpha_{Isc}(T_c - T_o)\right] \tag{3.1}$$

$$I_{mp} = I_{mpo}[C_0 E_e + C_1 E_e^2][1+\alpha_{Imp}(T_c - T_o)] \tag{3.2}$$

$$V_{oc} = V_{oco} + N_s \delta(T_c)\ln(E_e) + \beta_{Voc}(E_e)(T_c - T_o) \tag{3.3}$$

$$V_{mp} = V_{mpo} + C_2 N_s \delta(T_c)\ln(E_e) + C_3 N_s\left[\delta(T_c)\ln(E_e)\right]^2 + \beta_{Vmp}(E_e)(T_c - T_o) \tag{3.4}$$

$$P_{mp} = I_{mp} V_{mp} \tag{3.5}$$

$$FF = \frac{P_{mp}}{(I_{sc}V_{oc})} \tag{3.6}$$

where:

$$E_e = \frac{I_{sc}}{\left[I_{sco}\left\{1+\alpha_{Isc}(T_c - T_o)\right\}\right]} \tag{3.7}$$

$$\delta(T_c) = \frac{nk(T_c + 273.15)}{q} \tag{3.8}$$

$$\beta_{Vmp}(E_e) = \beta_{Vmpo} + m_{\beta Vmp}(1 - E_e) \tag{3.9}$$

Eq.(3.7), Eq.(3.8), and Eq.(3.9) represent the effective irradiance to which the photovoltaic cells in the modules can utilize, thermal voltage per cell at temperature T_c, and the thermal coefficient for the maximum power voltage as a function of E_e, respectively.

Additionally, two formulas Eq.(3.10) and Eq.(3.11) are included into the model to increase its versatility, by providing a better approximation to the I-V curve of the PV system, when the operating voltage used is different than the maximum power voltage. The first additional point I_x is calculated at half the open circuit voltage, and the second I_{xx} for a voltage that is the midpoint between V_{mp} and V_{oc}. The five points estimated using Sandia performance model seen on Fig. 8 recreate the basic shape of the I-V curve, they can be used to generate a new I-V curves for a different operating voltages, if required by the application.

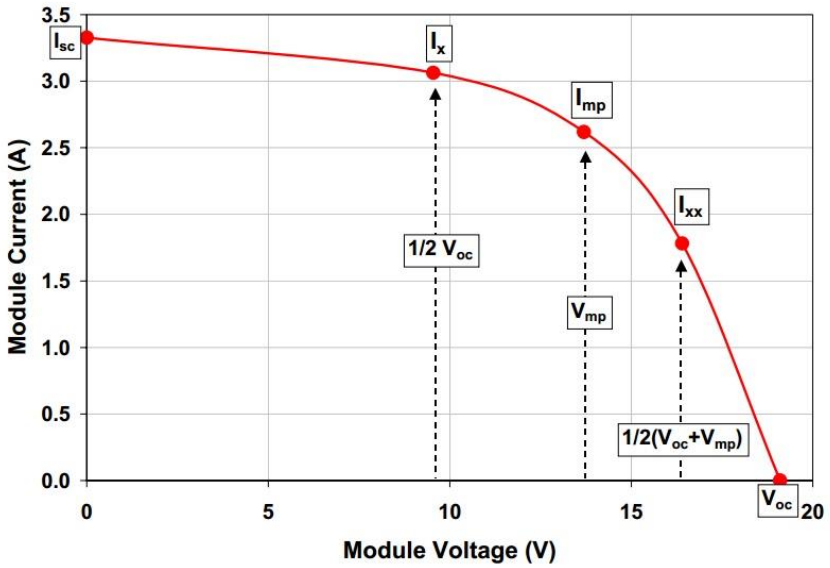

Fig. 8 Example of a module I-V curve with the five points calculated using the Sandia model, taken from [19]

$$I_x = I_{xo}\left(C_4E_e + C_5E_e^2\right)\left[1+\alpha_{Isc}(T_c - T_o)\right] \tag{3.10}$$

$$I_{xx} = I_{xxo}(C_6E_e + C_7E_e^2)\left[1+\alpha_{Imp}(T_c - T_o)\right] \tag{3.11}$$

For the simulation of arrays made out of many modules can be achieved by using Eq.(3.1) through Eq.(3.11), and accounting of the parallel and series combinations of the modules in the array. This can be done by multiplying the voltages calculated using Eq.(3.3) and Eq.(3.4) with the number of modules connected in series M_s. Additionally, the currents calculated using Eq.(3.1), Eq.(3.2), Eq.(3.10), and Eq.(3.11) with the number of modules connected in parallel in the array M_p. This approach ignores the resistance present in the system, due to the connecting wires, and the mismatch between the different modules, which leads to a little higher predicted performance, than the one produced in practice. The effect of the resistance and mismatch in general produces a difference of less than 5 (%) smaller, than the performance stated by the individual module stated nameplate ratings.

The model can be simplified by substituting Eq.(3.7) with Eq.(3.12), which is the most commonly used approach today to calculate the effective irradiance. This approach ignores the difference created by a mismatch of the solar spectral and angle of incidence, between the pyranometer(type of irradiance sensor) and photovoltaic array. Typically the error introduced by using Eq.(3.12) is in the range of 5 to 10 (%) error in measured irradiance.

$$E_e = \left(\frac{E}{E_o} \right) SF \tag{3.12}$$

B. Modeling of Li-ion Battery

To emulate the behavior of the battery a Battery dynamic model for electrical vehicle applications presented in [20] is used. The model is an electrical one, which accurately represents the electrical characteristics of batteries, and has been experimentally validated with four different battery types. The simplicity of the approach, allows for an easier extraction of the necessary battery parameters, which can be derived using three points of the manufacturer supplied discharge curve in steady state.

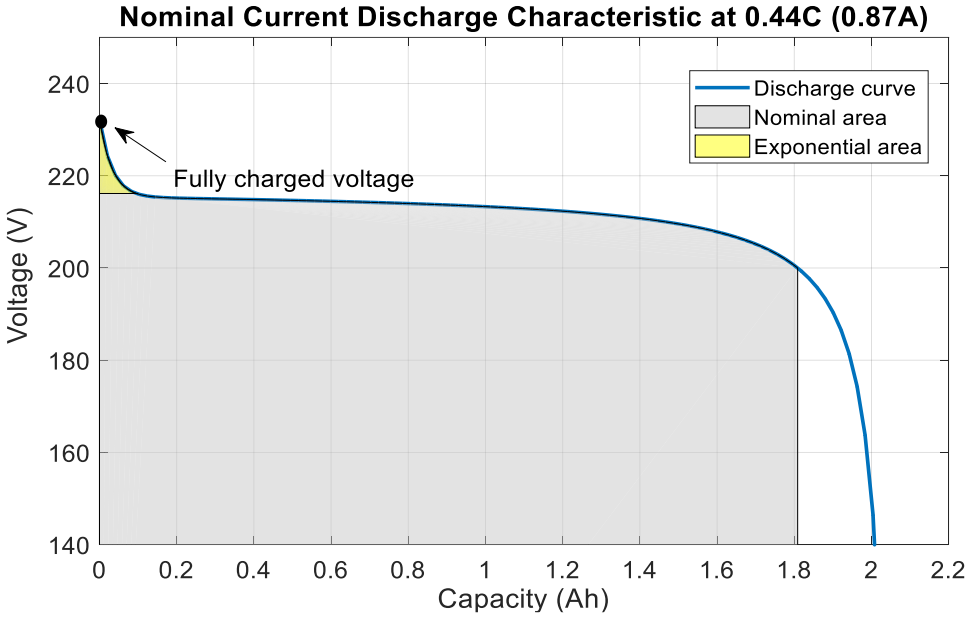

Fig. 9 Typical discharge curve

The typical discharge curve shown in Fig. 9 is for a Lithium-ion battery, taken for the 'power_battery' model in Simulink, showing its exponential and nominal areas. The model accurately recreates the voltage dynamics when the current varies, and includes the open circuit voltage (OCV) as a function of state of charge (SOC). The battery voltage can be estimated using Eq.(3.13), where $K\frac{Q}{Q-it}\cdot it$ represents the polarization voltage, $K\frac{Q}{Q-it}\cdot i^*$ the polarization resistance, and $Ae^{-B\cdot it}$ the exponential zone shown in Fig. 9. The exponential term

$$V_{batt} = E_0 - K\frac{Q}{Q-it}\cdot it - R\cdot i + Ae^{-B\cdot it} - K\frac{Q}{Q-it}\cdot i^* \tag{3.13}$$

in Eq.(3.13) is only valid for the Lithium-ion battery, for the remaining types like the Nickel-cadmium, Nickel-metal hydride, and Lead-acid the hysteresis phenomena between the charge and discharge, that is present has to be accounted for by Eq.(3.14) . The exponential voltage depends on its initial value $Exp(t_0)$ and the charging $u(t)=1$ or discharging $u(t)=0$ of the battery. The full discharge model can be seen in Fig. 10.

$$\dot{Exp}(t) = B\left|i(t)\right|\left(-Exp(t) + Au(t)\right) \tag{3.14}$$

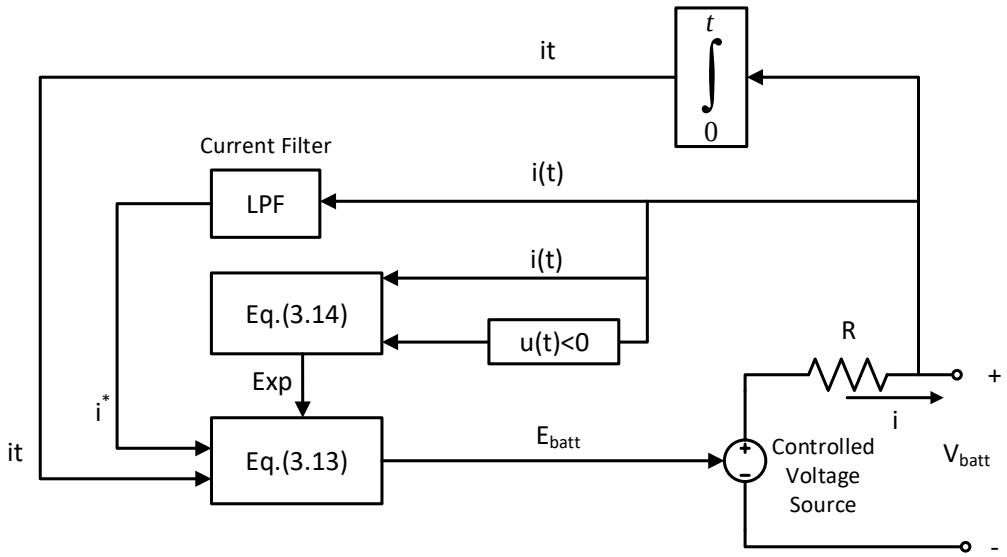

Fig. 10 Discharge battery model

Moving to the charging mode of the battery, where the characteristic at the end of charge (EOC) is different for the each battery type. The Lithium-ion and Lead-acid have identical EOC behavior, when the battery reaches the full state of charge the voltage increases rapidly. This is represented using the polarization resistance term, which during charging increases until the battery is almost full charged (it=0). For the charging case the polarization resistance in Eq.(3.13), has to be substituted with Eq.(3.15).

$$Polarisation\ Resistance = K\frac{Q}{it - 0.1Q} \tag{3.15}$$

For the Nickel-cadmium and Nickel-metal hydride the EOC characteristics are similar, but different than the one for Lithium-ion and Lead-acid batteries. The voltage starts to decrease slowly as a function on the current amplitude, after the battery has reached full charge voltage. This is again modeled by the polarization resistance, which is changed to Eq.(3.16) in Eq.(3.13) .

$$Polarisation\ Resistance = K\frac{Q}{|it| - 0.1Q} \tag{3.16}$$

All in all, accounting for the different behaviors of the batteries the final equations to emulate their performance are:

Lithium-ion

- Charge

$$V_{batt} = E_0 - K\frac{Q}{Q - it}\cdot it - R\cdot i + Ae^{-B\cdot it} - K\frac{Q}{it - 0.1\cdot Q}\cdot i^* \tag{3.17}$$

- Discharge

$$V_{batt} = E_0 - K\frac{Q}{Q - it}\cdot\left(it + i^*\right) - R\cdot i + Ae^{-B\cdot it} \tag{3.18}$$

Lead-acid

- Charge

$$V_{batt} = E_0 - K\frac{Q}{Q - it}\cdot it - R\cdot i + Exp(t) - K\frac{Q}{it - 0.1\cdot Q}\cdot i^* \tag{3.19}$$

- Discharge

$$V_{batt} = E_0 - K\frac{Q}{Q - it}\cdot\left(it + i^*\right) - R\cdot i + Exp(t) \tag{3.20}$$

Nickel-cadmium and Nickel-metal hydride

- Charge

$$V_{batt} = E_0 - K\frac{Q}{Q - it}\cdot it - R\cdot i + Exp(t) - K\frac{Q}{|it| - 0.1\cdot Q}\cdot i^* \tag{3.21}$$

- Discharge

$$V_{batt} = E_0 - K\frac{Q}{Q - it}\cdot\left(it + i^*\right) - R\cdot i + Exp(t) \tag{3.22}$$

The following number of assumptions are made in the model:

- The internal resistance is considered constant during the operation of the modal for both cases of charging and discharging.

- The parameters taken for the discharging curve to create the model are assumed to be the same for the charging case.
- Battery capacity remains constant, and is not affected by the amplitude of the current.
- The effect of temperature is not taken into account by the model.
- The Self-Discharge effect is not modeled.
- The battery does not exhibit a memory effect.

Additionally, the limitations inherent in the model are, the minimum open circuit voltage is 0 (V) and the maximum voltage for the battery is $2*E_0$, further the SOC cannot be greater than 100 (%) when the battery is overcharged. The maximum capacity is Q, while the minimum is 0 (Ah) for the battery.

Chapter 4 Evaluation of Smoothing Methods – Simulation

To evaluate the smoothing strategies irradiance data for three different days in Aalborg, Denmark, a day with clear sky taken on 24.07.2012 shown in Fig. 11, a day with high irradiance variability due to fast moving clouds from 23.09.2012 plotted in Fig. 12, and a day with even highest variation of irradiance on 23.07.2012 displayed in Fig. 13. The irradiance data is reduced for the 24 hours to remove the period during the night, where no power is produced, and further reduction of the sunrise and sunset periods are made to make the irradiance profile easy to evaluate. Below the irradiance plot is the ramp rate produced by the PV panels as a percentage of its maximum power, with no smoothing included. This allows for a clear comparison between the three days presented.

The simulation consists of PV array modeling of BP Solar MSX120 modules, 8 of them connected in series to produce maximum power of 960 (W) with parameters shown in Table 1. Additionally, a Lithium-ion battery is simulated with nominal voltage 200 (V), and a total capacity of 2.0 (Ah), the parameters of the battery are taken from the 'power_battery' model in Simulink and are shown in Table 2. As already mentioned in the beginning of chapter 3 the converters are omitted, and the power produced by PV model and battery model are added to produce the active power supplied to the grid Fig. 14.

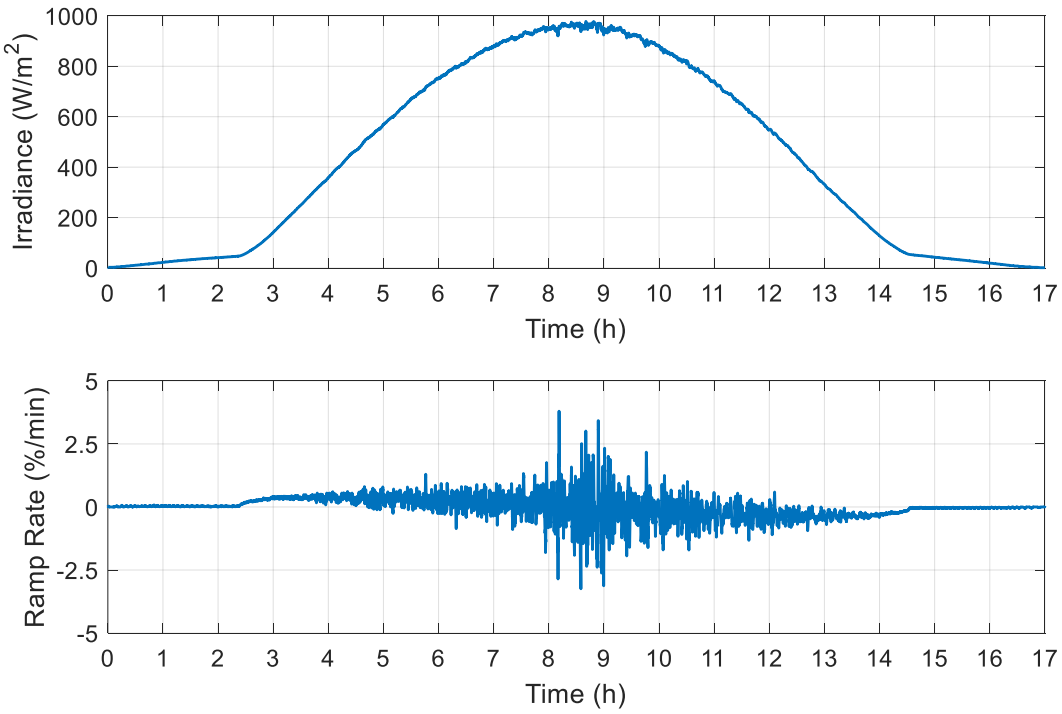

Fig. 11 Clear sky day and its ramp rate profile

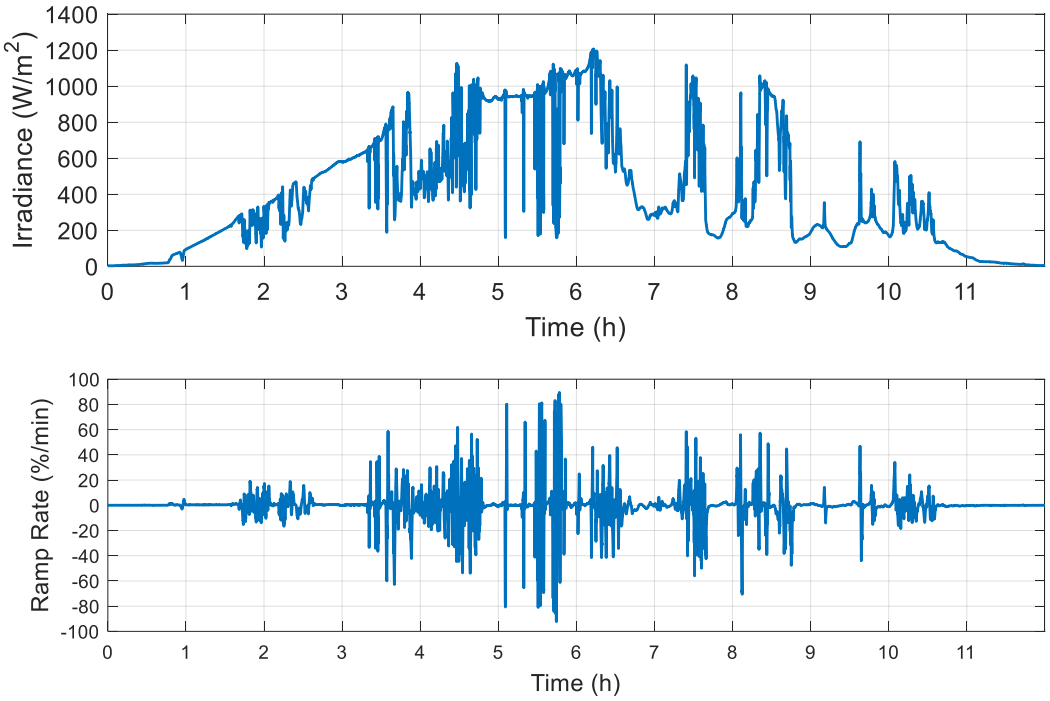

Fig. 12 High variation of irradiance day and its ramp rate profile

Table 1 Parameters of PV module

BP Solar MSX120 single module	
Maximum Power ($P_{\max}$)	120 (W)
Voltage at $P_{\max}$ (V_{mp})	33.7 (V)
Current at $P_{\max}$ (I_{mp})	3.56 (A)
Minimum $P_{\max}$	114 (W)
Short-circuit current (I_{sc})	3.87 (A)
Open-circuit voltage (V_{oc})	42.1 (V)
Temperature coefficient of (I_{sc})	0.0065±0.015 (%/°C)
Temperature coefficient of (V_{oc})	-80±10 (mV/°C)
Temperature coefficient of power	-0. 5±0.05 (%/°C)

To evaluate the smoothing methods the following criteria will be used:

- Does the method guarantee that the ramp rate limit of 10 (%/min) of maximum PV power will be followed in all cases
- The amount of energy used per hour
- The peak instantaneous power needed
- How is the battery utilized and what is its state at the end of the day

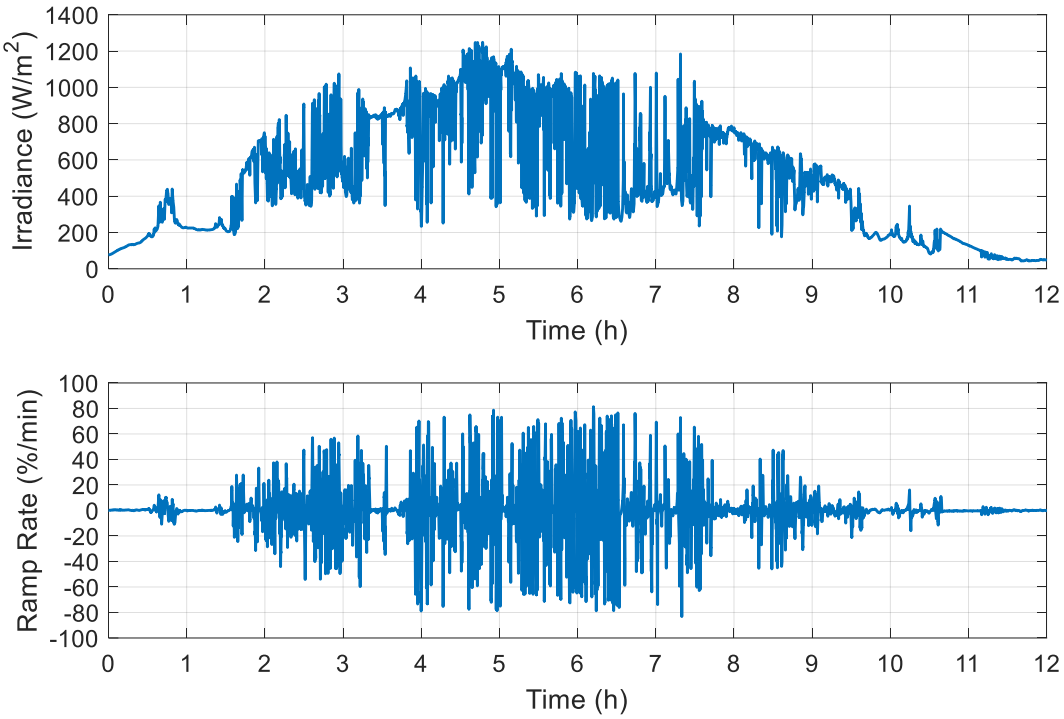

Fig. 13 Highest variation of irradiance day and its ramp rate profile

Table 2 Parameters of battery stack

Lithium-ion battery	
Nominal voltage (V_{nom})	200 (V)
Constant voltage (E_0)	216.8718 (V)
Internal Resistance (R)	1 (Ω)
Polarization constant (K)	0.74918 (V/(Ah))
Exponential zone amplitude (A)	16.7952 (V)
Exponential zone time constant inverse (B)	30.531 $(Ah)^{-1}$
Response time (T_r)	30 (s)
Maximum capacity (Q)	2.0 (Ah)
Fully charged voltage (V_{full})	232.7974 (V)

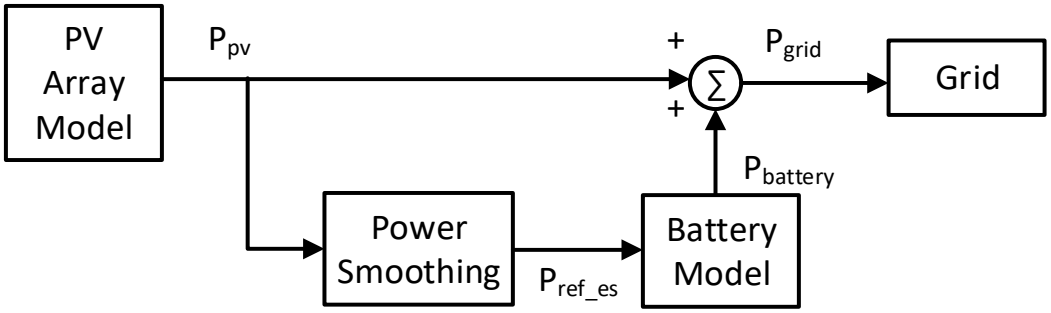

Fig. 14 Simulation model structure

A. First Order Low Pass Filter Method

For tuning the LPF the highest irradiance variation day will be used as a reference, such that the tuned filter will produce a battery power reference to diminish the ramp rate variations to the limit of 10 (%) of maximum PV power per minute. The proposed filter time constant of 2 (min) in [13], proved insufficient to limit the grid variation to 10 (%/min), so a new value needed to be located. The procedure to find it is as follows, first the filter time constant is set to an initial value, for example the proposed 2 (min), and then the simulation of the system is performed, at which point from the ramp rate figure it can be seen if the 10 (%/min) limit is violated. The filer time constant is adjusted iteratively until the ramp rate of the grid power is below the limit. The highest day variation in irradiance is used as a reference during the tuning presented in Fig. 13. The final can be seen in Fig. 15, where the filter time constant of $T_f = 360$ (s) is used.

In Fig. 16 the same filter settings are used, however it can be noted that the 10 (%/min) limit is violated for the period of a minute. This confirms the statement made in chapter 2 that the filter cannot guarantee that the ramp rate will not be violated. When retuning the filter again, a suitable time constant of $T_f = 425$ (s) is found, for the high variation in irradiance day, which results in no violations in the limit. To overcome this problem it is recommended that data with the highest peak ramp rate variation is used to perform the tuning process, if the limit has to be followed without exception. The battery power provided to smooth the PV power fluctuations accompanied by the SOC of the battery, is also present in Fig. 16. From the profile of the SOC it can be noted that at the end of the day the battery returns within 2 (%) of the initial SOC, which in this simulation is 50 (%). This is a positive since only a small amount of power is needed to return the battery in the initial condition for the next day.

By comparing the ramp rate of clear sky day present in Fig. 17 and the one in Fig. 11 it can be seen that the PV power fluctuations are smoothed by the filter, even though they are below the limit for the whole day. Ideally the battery will not be used when the variations in power are below the requirement of 10 (%/min), since its lifetime will be reduced.

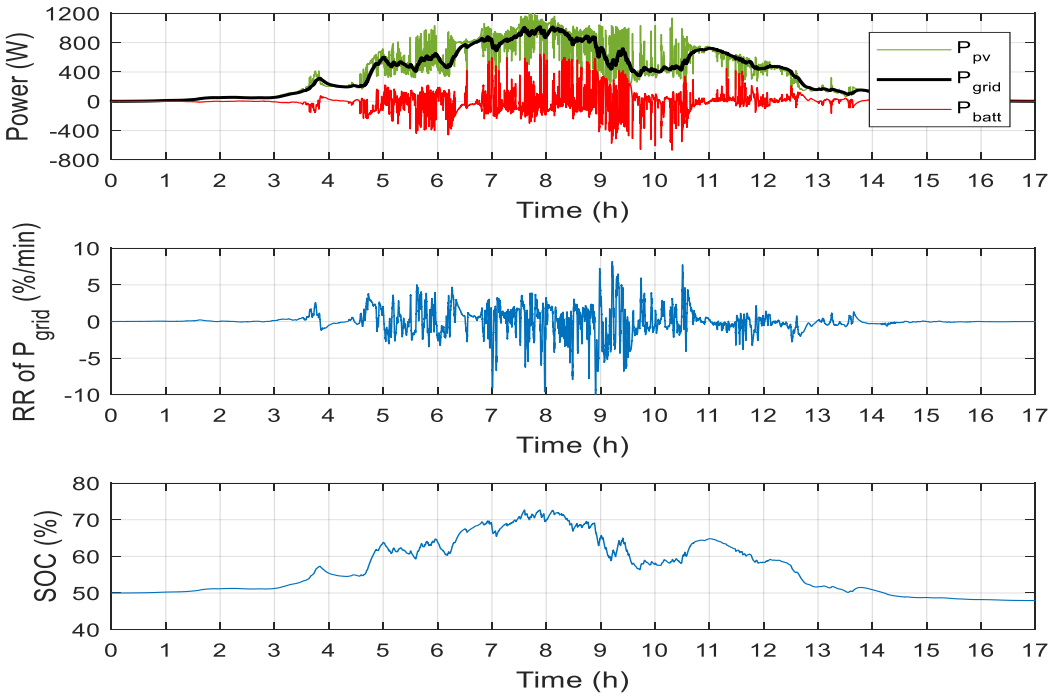

Fig. 15 LPF smoothing in highest irradiance variation day

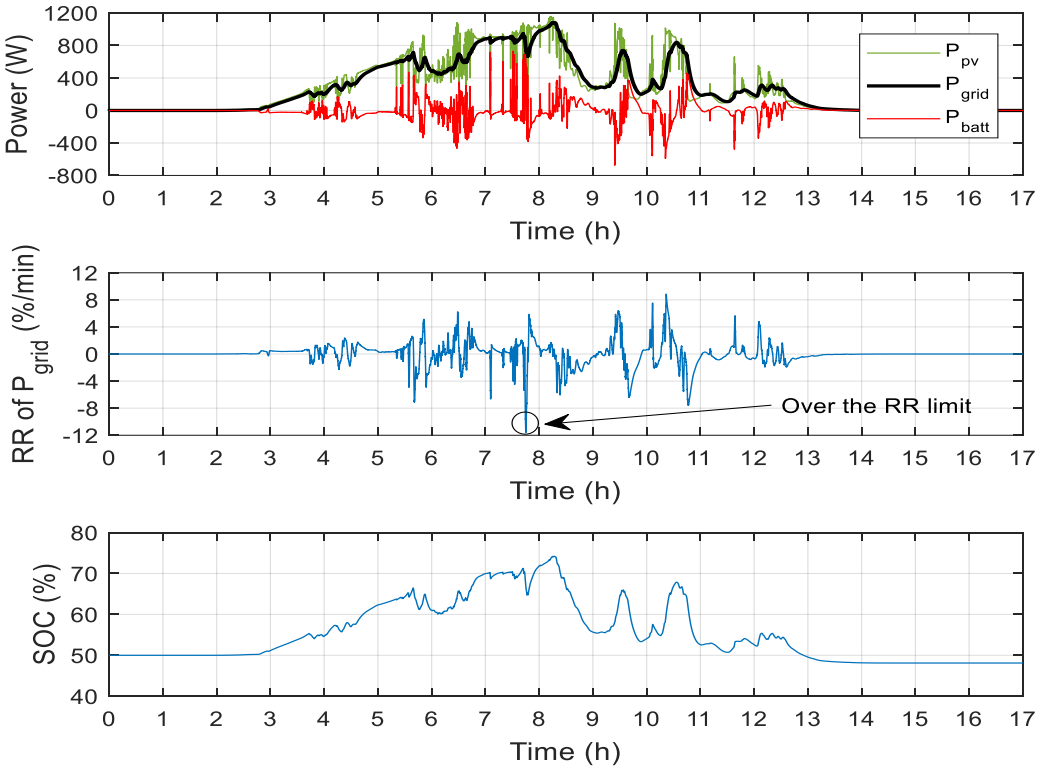

Fig. 16 LPF smoothing in high irradiance variation day

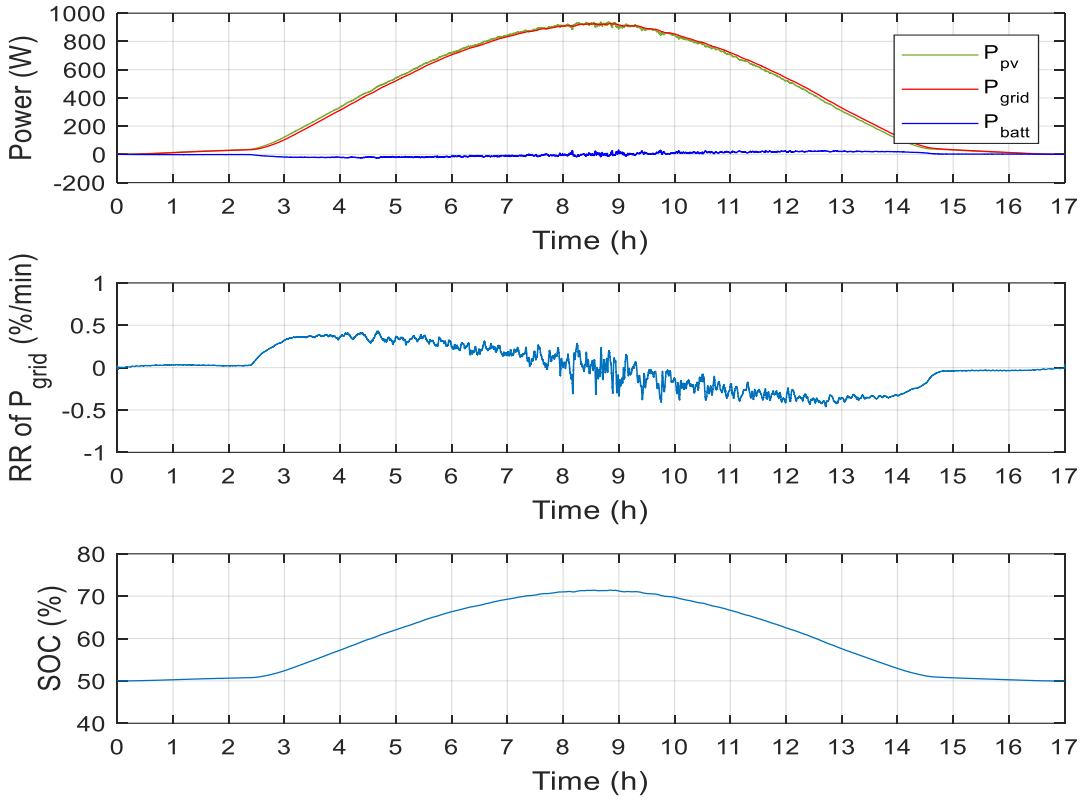

Fig. 17 LPF smoothing in a clear sky day

B. Ramp Rate Control Based on Gradient Method

1. Original Gradient Design

During the implementation of the gradient method from [8] a few problems were encountered. In the paper they state that "$\left.\frac{dP_{grid}}{dt}\right|_{des}$ is the desired ramp rate that of the PV inverter, which will be negative during a ramp-down event and positive during a ramp-up event.", which can be implemented two different ways shown in Eq.(4.1) and Eq.(4.2). The result of implementing the rule both ways can be noted in Fig. 18, where Eq.(4.1) is implemented in subplot a) and Eq.(4.2) shown in subplot b).

$$\left.\frac{dP_{grid}}{dt}\right|_{des} = \begin{cases} \left|\left.\frac{dP_{grid}}{dt}\right|_{des}\right|, & \text{if } \frac{dP_{pv}}{dt} > 0 \\ -\left(\left.\frac{dP_{grid}}{dt}\right|_{des}\right), & \text{otherwise.} \end{cases} \tag{4.1}$$

$$\left.\frac{dP_{grid}}{dt}\right|_{des} = \begin{cases} -\left(\left.\frac{dP_{grid}}{dt}\right|_{des}\right), & \text{if } \frac{dP_{pv}}{dt} < 0 \\ \left|\left.\frac{dP_{grid}}{dt}\right|_{des}\right|, & \text{otherwise.} \end{cases} \tag{4.2}$$

It can be noted that the battery is being charged in a), and discharged in case b), when the PV power is zero, i.e. $\frac{dP_{pv}}{dt} = 0$, and does not vary after the three and a half minutes. This will lead to either the overcharging or discharging the battery, and will damage it.

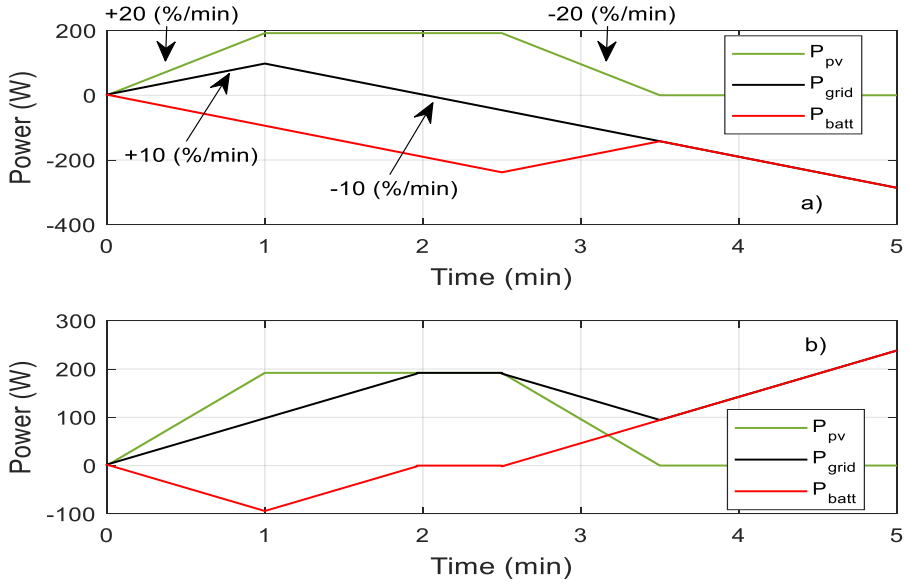

Fig. 18 Gradient method initial implementation

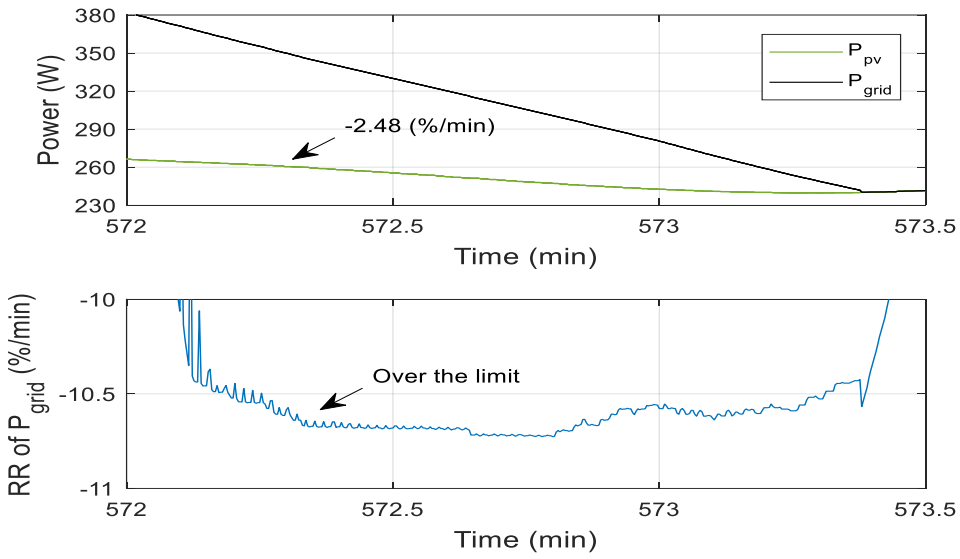

Fig. 19 Gradient method limit issue

After the above complication was solve, a separate issue arose, which is that the ramp limit is not always met as displayed in Fig. 19, where the highest variation of irradiance day is used for the simulation. The ramp rate of the PV power is seen to be only -2.48 (%/min), which is below the ±10 (%/min). The grid power according to the gradient approach should be going down at -10 (%/min), but since a dead zone Eq.(2.6) is present some of the variations of P_{pv} are added to the -10 (%/min) slope, leading to a gradient higher than is needed for the duration of a minute. The authors of this approach stress, that one of the biggest advantages of this method is that it guarantees that the ramp rate limit will be followed in all cases, as compared to other methods, which does not seem to be the case here with the irradiance profile used. Proposed ways to solve these problems are presented in the next subsection.

2. Proposed Modification to Gradient Method

To solve the problem of giving the wrong sign to $\left.\frac{dP_{grid}}{dt}\right|_{des}$, when at $\frac{dP_{pv}}{dt}=0$ an additional case was added to Eq.(4.1), which gives the correct sign as seen in Eq.(4.3). The result of this change is shown in Fig. 20, where the approach now tends to lead the grid ramp rate in such a way as to the minimize the use of battery power, while the ramp limit is fulfilled. The PV power has a slope of 20 (%/min) in the beginning and (%/min) at the end between 2.5 and 3.5 (min) in Fig. 20, and that P_{grid} takes twice as long to match the P_{pv} at both ends, thus the gradient of the grid power is half of the 20 (%/min).

$$\left.\frac{dP_{grid}}{dt}\right|_{des} = \begin{cases} \left|\left.\frac{dP_{grid}}{dt}\right|_{des}\right|, & \text{if } \frac{dP_{pv}}{dt} > 0 \\ \left|\left.\frac{dP_{grid}}{dt}\right|_{des}\right|, & \text{elseif } \frac{dP_{pv}}{dt} = 0 \text{ and } P_{batt} < 0 \\ -\left(\left.\frac{dP_{grid}}{dt}\right|_{des}\right), & \text{otherwise.} \end{cases} \tag{4.3}$$

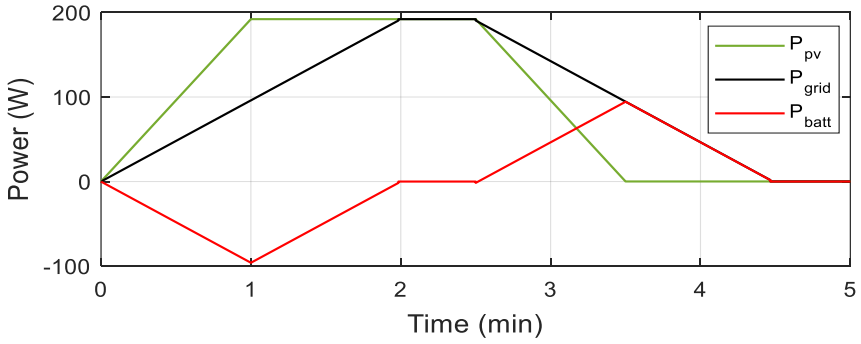

Fig. 20 Gradient method proposed implementation

Additionally once the power of the battery goes below $\left.\frac{dP_{grid}}{dt}\right|_{des}$, the dead zone is activate, with the switching function leading to a zero reference power being supplied to the battery model.

For the issue of violating the ramp rate discussed in the previous subsection, a change of the dead zone in Eq.(2.6) is proposed to eliminate it, which is presented in Eq.(4.4), were the $P_{battery}$ is added as an additional reference for when the dead band can be activated.

$$f\left(\frac{dP_{pv}}{dt}\right)=\begin{cases}0, & \text{if } \eta_{inv}\left[\frac{dP_{pv}}{dt}\right]\leq\left.\frac{dP_{grid}}{dt}\right|_{des} \text{ and } \left|P_{battery}\right|<\left.\frac{dP_{grid}}{dt}\right|_{des}\\ \frac{dP_{pv}}{dt}, & \text{otherwise.}\end{cases} \tag{4.4}$$

The resulting change leads to a stricter following of the ramp rate limit as is displayed in Fig. 21, there are some violations of the limit, but they are for a insignificantly small duration of 1 or 2 times the sampling period, thus they can be neglected.

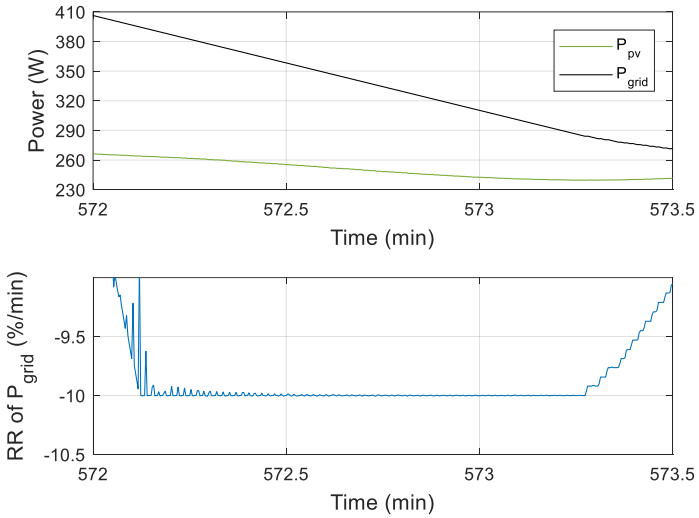

Fig. 21 Gradient method additional refinement

Now that the method is working properly we can start to evaluate its performance. First, in Fig. 22 it can be noted that there are indeed periods during which the PV power increase or decreases, with a ramp rate below the limit, and the battery in those cases is not used. This can be seen even more clearly in Fig. 22 and Fig. 23, where the battery is not used for some periods of time, as noted by the zero battery power, which confirms that the dead zone introduced is working as intended. Another advantage to the method, compared with the LPF approaches, is that it does not require to be retuned, for example in a day with steeper ramp rates than the one presented in Fig. 22 and Fig. 23 will works equally well, there is no additional need to modify it. For all three days the required 10 (%/min) gradient is followed. Additionally, it can be seen in Fig. 22 and Fig. 23 that in the ramp rate plot the variations are much closer to the limit compared with Fig. 15 and Fig. 16, which means that the smoothing provided by this method is less aggressive compared to the previously presented LPF.

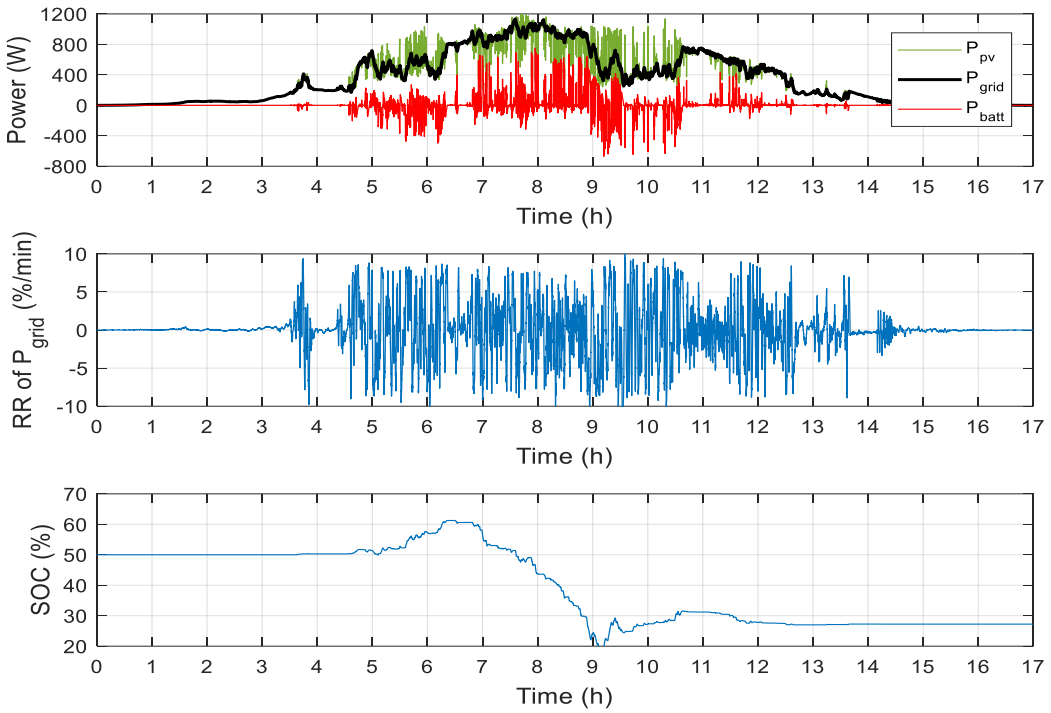

Fig. 22 Gradient method smoothing in highest irradiance variation day

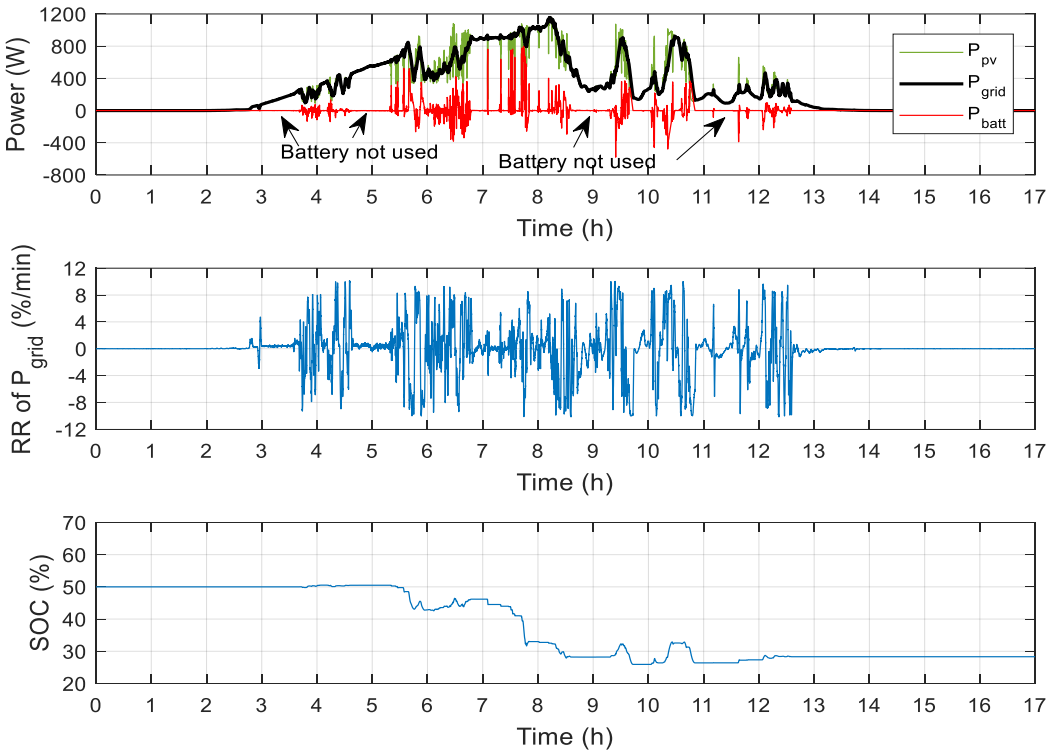

Fig. 23 Gradient method smoothing in high irradiance variation day

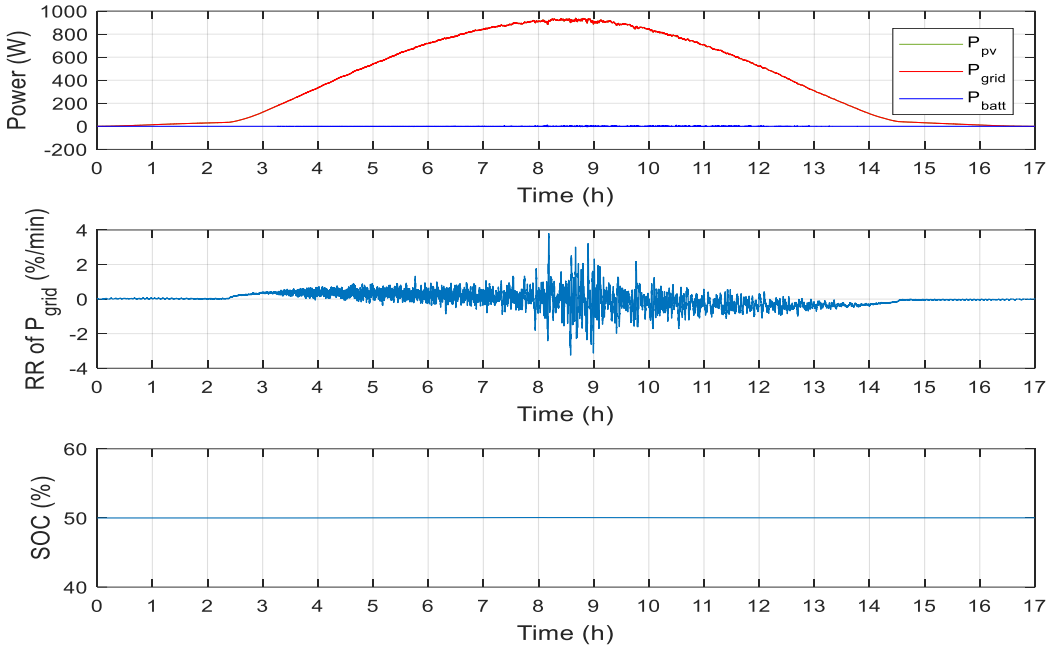

Fig. 24 Gradient method smoothing in a clear sky day

The downside of the gradient approach can be noted in the final value for state of charge at the end of the day both in Fig. 22 and Fig. 23. For both days the battery is left with around 28 (%) SOC, which means that for the next day the battery has to be charged from the grid. Compared with the first order LPF where only 2 (%) of battery power has to be provided to return the batter to initial value of 50 (%) SOC. This is undesirable, since the energy purchased from the grid is expensive compared to the energy produced by the PV system, which is free, not considering the initial investment. Depending on the ratio of clear sky days to days with large amount of clouds, i.e. high variation in irradiance, in certain cases the benefit of not using the battery during a clear sky day may outweigh the disadvantage of having to charge the battery from the grid.

C. Proposed Second Order Low Pass Filter Method

The tuning process is the same as for the first order low pass filter, the damping ratio $\zeta = 0.707$ is chosen, since this leads to neither the amplifying nor dampening of the input before the natural frequency w_n. Again the reference data for the tuning process show in Fig. 13 is used, because this way a comparison between the filter results can be made under the same conditions. This will allow for an objective assessment of the advantages and disadvantages of the smoothing methods presented in the next section.

.

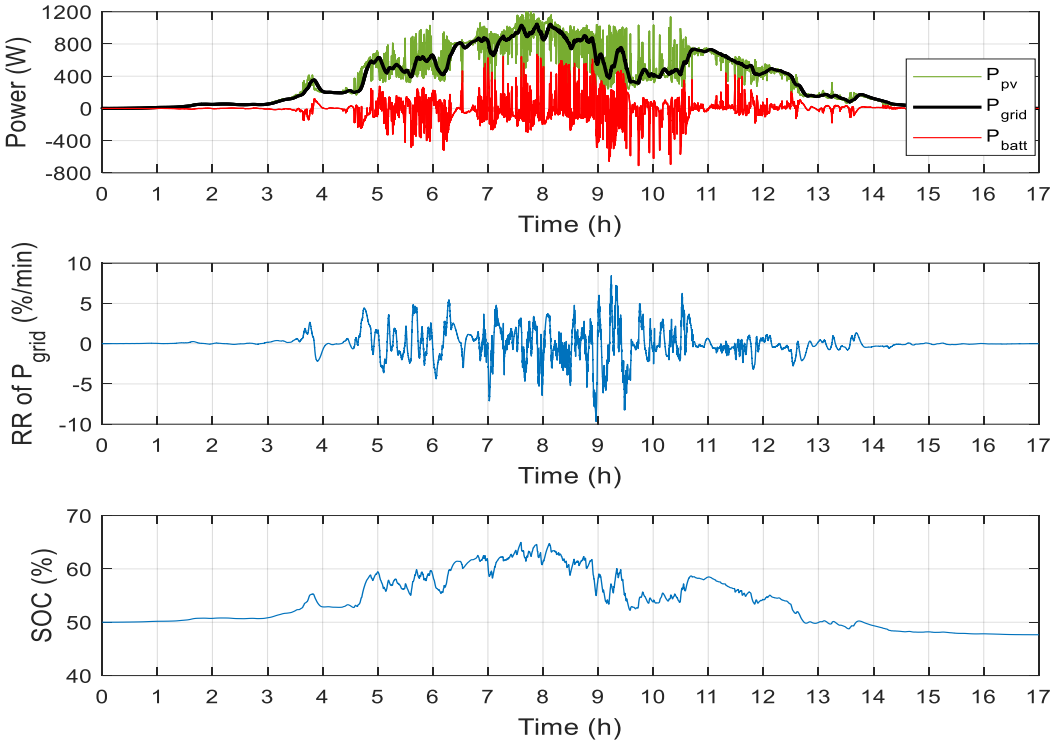

Fig. 25 LPF smoothing in highest irradiance variation day

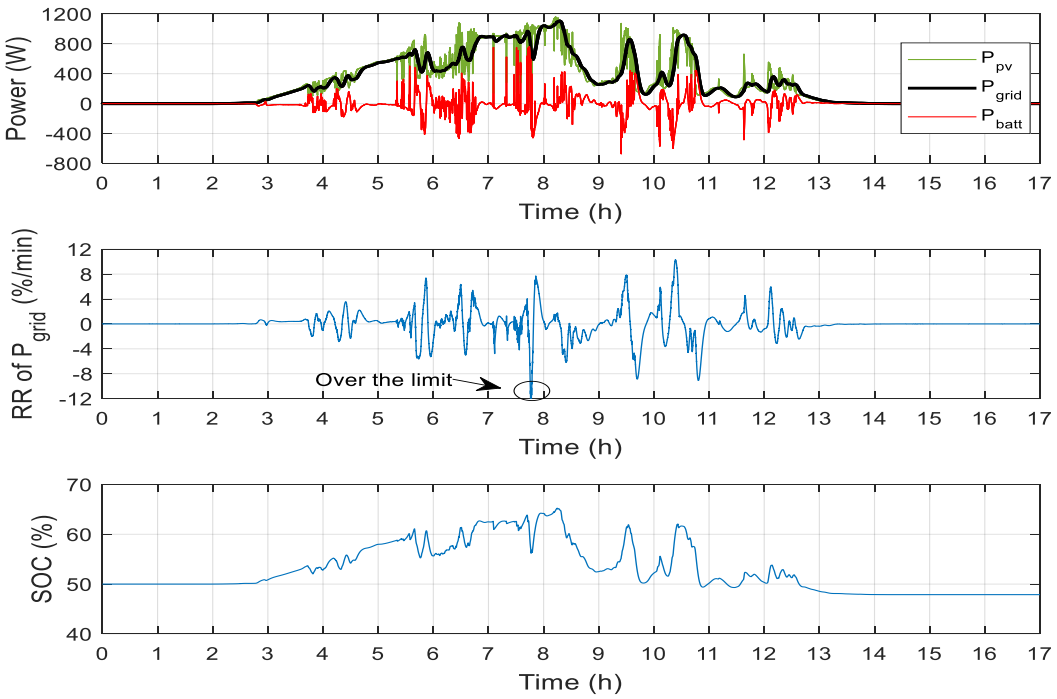

Fig. 26 LPF smoothing in high irradiance variation day

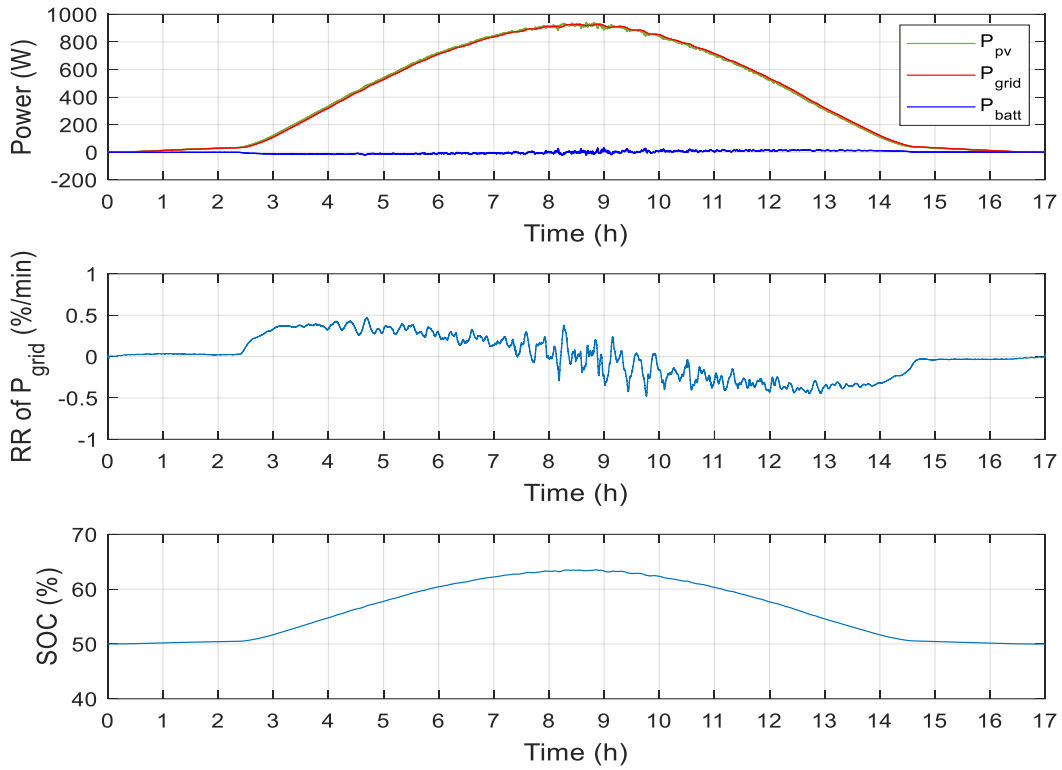

Fig. 27 LPF smoothing in a clear sky day

The natural frequency of $w_n = 1/160\,(rad/s)$ is found to keep the PV power fluctuations below the limit of 10 (%/min). This is true for both the data in Fig. 25 and Fig. 27 and not correct in Fig. 26, mirroring the results from the first order low pass filter. To solve this problem the filter has to be made more aggressive by decreasing w_n to the value of $1/190\,(rad/s)$. Similarities can be noted in the state of charge plots for all three days, between both filters in that the SOC is more or less returns to 2 (%) of its initial value of 50 (%) at the end of the day

During the clear sky day Fig. 27 the battery is used, when the situation does not require it, because the ramp rate of the PV power for the whole day is below the limit as displayed in Fig. 11. The battery is slowly charged for the period of five and a half hours until it reaches a charge of 63 (%), then it is discharged for the next 5 hours returning to the starting SOC value.

D. Comparison Between the Different Smoothing Methods and Battery Sizing

Let us compare the grid power signals produced by the smoothing approaches for the highest and the high variation of irradiance days presented in Fig. 28 and Fig. 29, where we have focused on a 2 hour section of data in the plots for clarity. From the graphs it can be seen that the smoothing by the gradient method (GM) is the least aggressive, since the distance between the peaks and the valleys is the most significant of the three. The second order low pass filter (LPF_{2nd}), is located more or less between the first order low pass filter (LPF_{1st}) and gradient method, which means it is more aggressive than the former and less aggressive than the latter approaches. The most smoothed grid power curve is due to the first order filter.

Similar to the conclusions in the above paragraph can be made if we look at the ramp rate of for the same periods of time presented in Fig. 30 and Fig. 31. The ramp rates of the gradient method's grid power go closer to the limit than the other two schemes, which means that less power is either charged or discharged from the battery for smoothing. The difference in the filter methods is not that pronounced, however it is safe to say that the ramp rate is closer to the limit for the second order LPF particularly in Fig. 30, around the 6.05 (h) and 6.35 (h) marks and in Fig. 31, near 9.5 (h) and 9.7 (h). The low pass filter again is shown to keep the variations in grid power morel close to zero that the other two approaches.

The energy curves for all three approaches are displayed in Fig. 32, Fig. 33, and Fig. 34, accompanied by the state of charge curves to make it clear, when power is flowing in and out of the battery. First it can be noted that the energy curves for the filters are to some extend symmetrical if bisected in the vertical plane of the graphs plane for all three figures. However the gradient method has quite a different pattern of power flow, and more energy is taken out of the battery shown in Fig. 32 and Fig. 33.

From the energy curves presented in Fig. 32, we find that for the highest variation in irradiance day, 88 (Wh) of energy have been taken from the batter by the end of the day, by the gradient smoothing approach. For the high variation in irradiance day Fig. 33, only 87 (Wh) have been used, while for the clear sky day the battery is not used at all. Looking at the filter methods, both have charged and discharged the battery with and almost equal amount of energy for the days, shown in Fig. 32, Fig. 33, and Fig. 34. This is an advantage compared with the gradient method, since very little charging of the battery has to be done before the system is ready for the next day of operation.

If we look at Fig. 32, Fig. 33, and Fig. 34. , we can see the peak energy charged and discharged from the battery. It can be noted that the power used by the second order LPF for all three cases is less than the one for the first order filter. This is also evident looking at the SOC plot, where we can see that the battery is used less by the second order filter. The gradient method on the other hand uses more charge for a shorter period of time, since the method does not delay the signal as the low pass filters do.

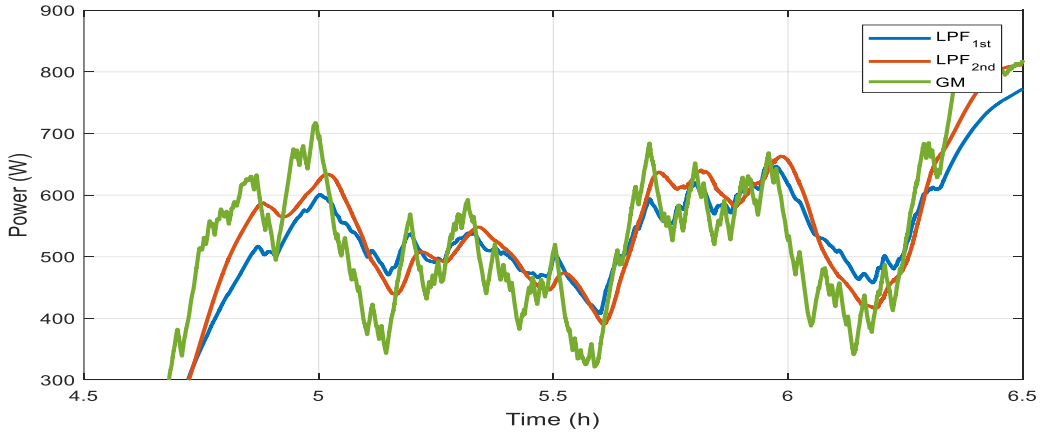

Fig. 28 Grid power curves produced by smoothing methods during highest irradiance variation day

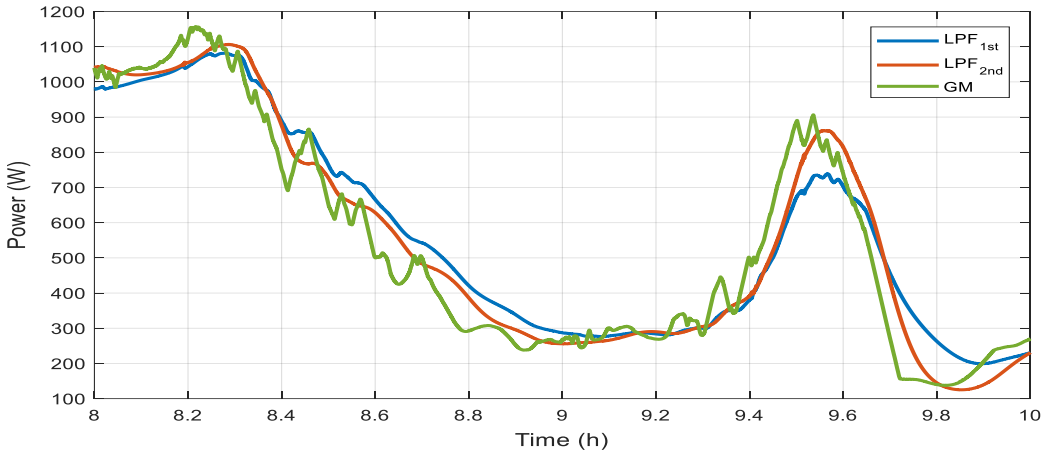

Fig. 29 Grid power curves produced by smoothing methods during high irradiance variation day

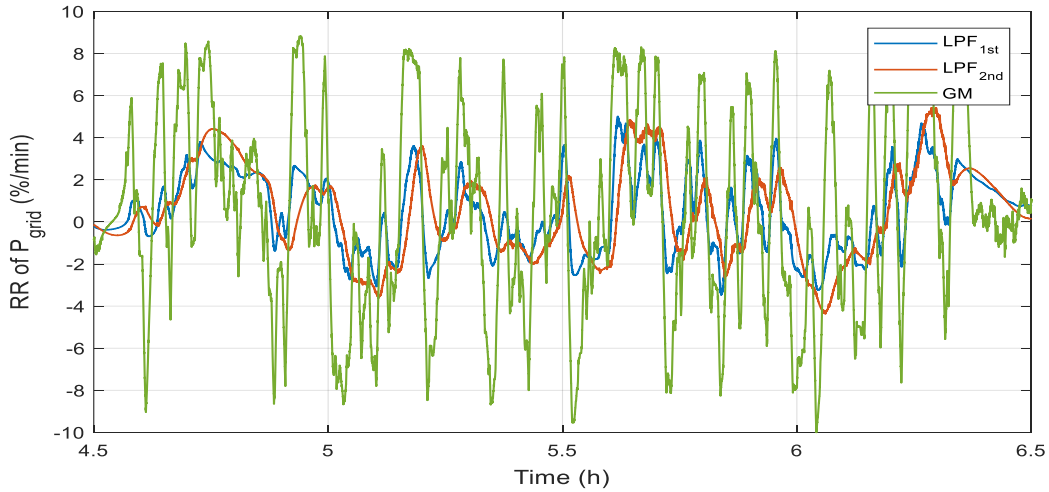

Fig. 30 Ramp rate of grid power curves produced by smoothing methods during highest irradiance variation day

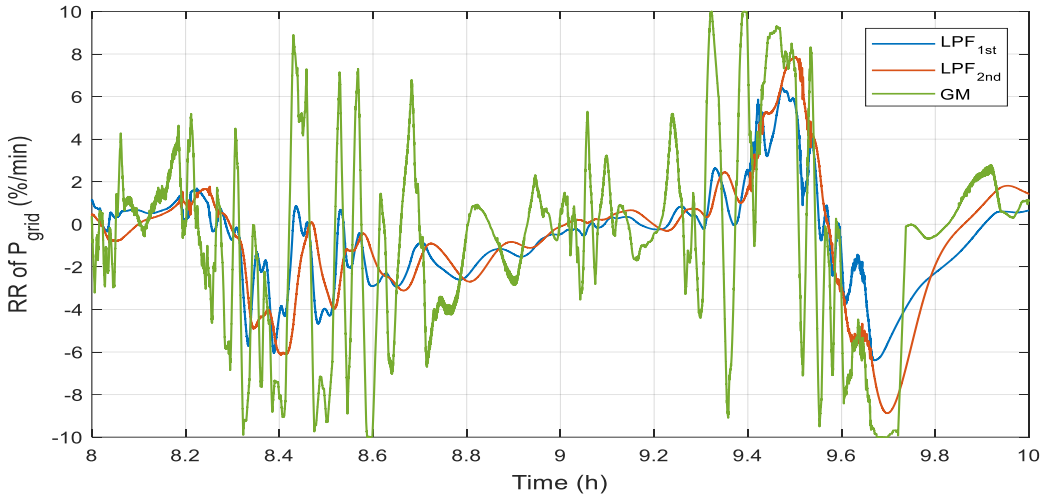

Fig. 31 Ramp rate of grid power curves produced by smoothing methods during high irradiance variation day

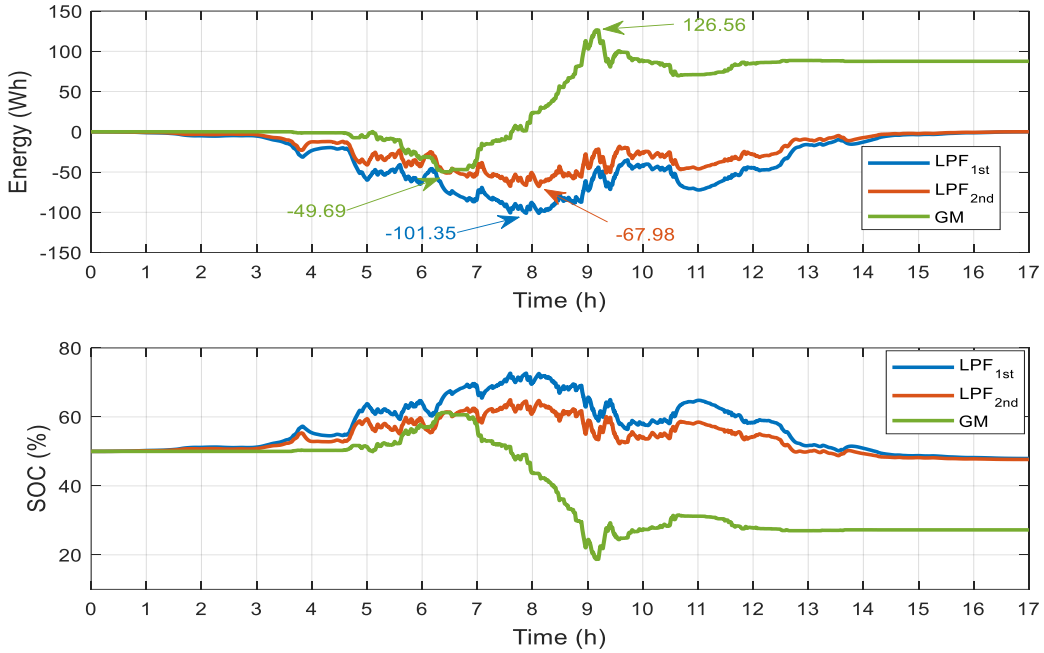

Fig. 32 Energy and SOC used by the smoothing methods during highest irradiance variation day

This difference battery usage is most noticeable in Fig. 34, between the LPFs and gradient method, since the battery will not be used during a clear sky day leading to its longed lifetime for the latter, while for the filter approaches at least the expenditure of energy is reduced in comparison with Fig. 32 and Fig. 33.

By comparing the first order and second order filters in Fig. 33, we can see that the energy needed is reduced from 108.2 (Wh) to 70.5 (Wh). Similar differences are noted in Fig. 32 and Fig. 34 possible due to the steeper magnitude gradient of the Second order filter noted in Fig. 35.

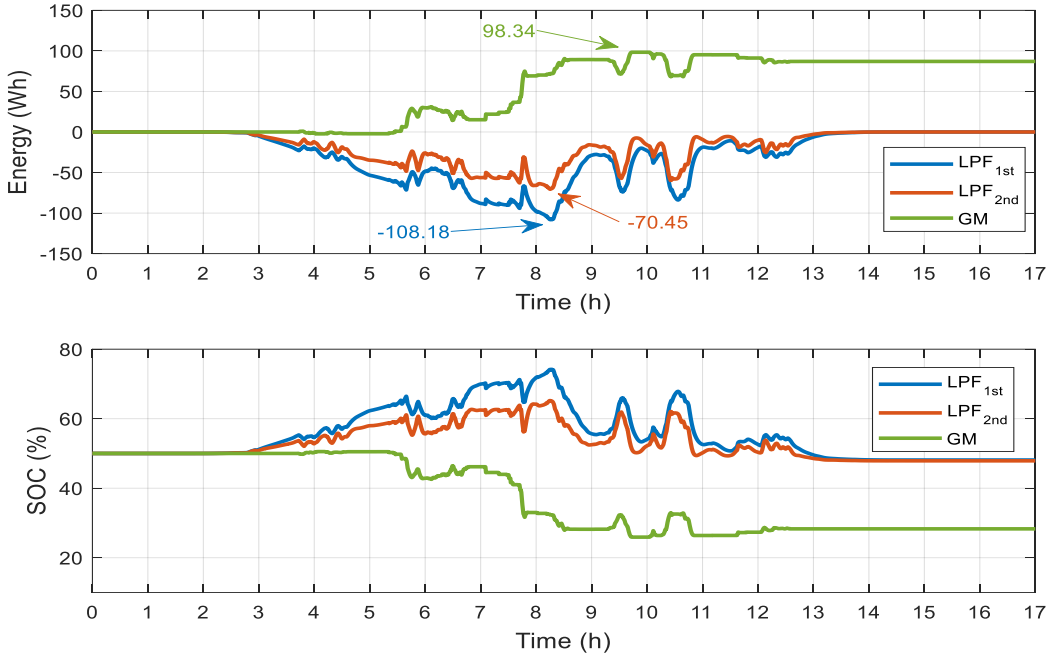

Fig. 33Energy and SOC used by the smoothing methods during high irradiance variation day

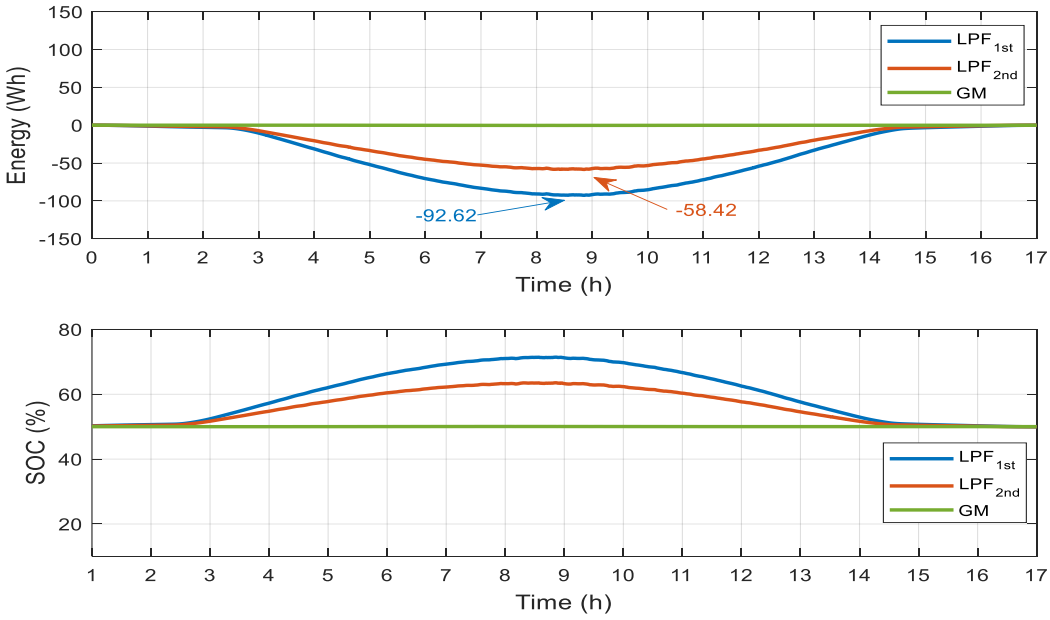

Fig. 34 Energy and SOC used by the smoothing methods during clear sky day

The area between the second order transfer function magnitude curve and the first order indicated with an arrow, shows that the second order filter attenuation of the input signal is less than the other filter before the two lines intersect. This means that more of the low frequencies are bypassed by the second filter, which may point to a similar effect happening with the ramp rates. This will explain the less aggressive smoothing and the less energy used by the second order filter mentioned before.

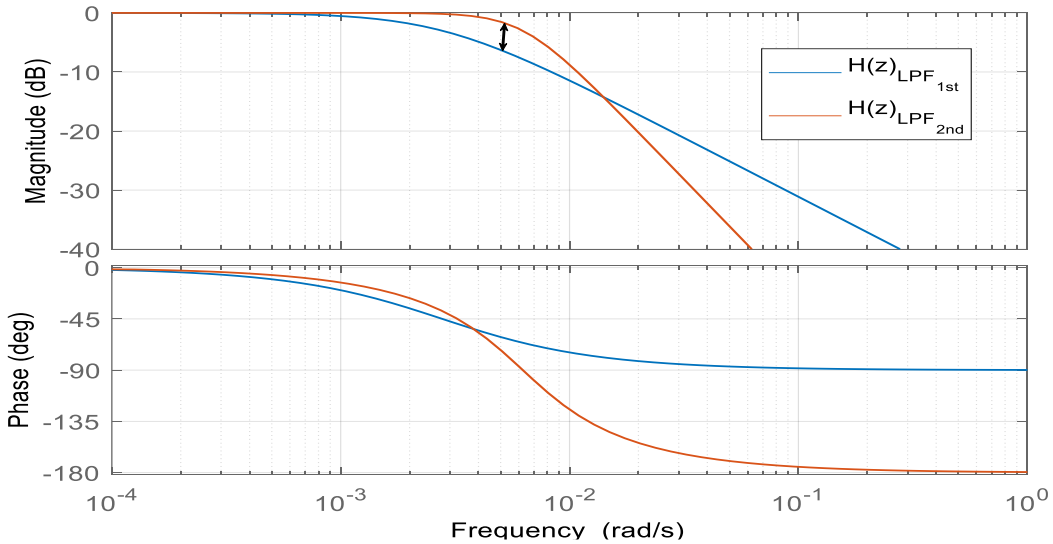

Fig. 35 Bode diagram of first and second order low pass systems

Finally we will briefly discuss how the battery size can be determined for the energy curve presented. In [21] a detailed theoretical of what size battery is needed according to the different ramp rate limits and a cost benefit analysis. In this report however we present a much simpler approach to calculate the battery size based on the energy consumed by the smoothing methods. It is generally recommended to use the battery from 20 to 80 (%) state of charge, as to extend its lifetime. For the above statement we have a remaining 60 (%) SOC to use during the day for power smoothing. If we look at Fig. 33 we can see that for the filters the energy starts from 0 and goes to maximum peaks of -108.18 (Wh) and -70.45(Wh), which means that these values can be directly used as E_{peak} to calculate the battery size. For the gradient method, since we have in the peak energy in Fig. 32 is taken $E_{peak} = 128.59 + \left|-49.69\right| (Wh)$ .Using Eq.(4.5), we can calculate the minimum battery size needed for all smoothing methods, where the assumption is made that E_{peak} is the most amount of power that will be consumed in a day for the whole year. For the filter approaches the initial state of charge is assumed to be 25 (%), leaving 5 (%) SOC to account for the small discharge at the end of the day mentioned in pervious sections. Since in Fig. 32, Fig. 33, and Fig. 34, the filter methods first charge the battery for half the working period and then discharge it for the rest. This means that we can start at low SOC and used the full range of the battery until 80 (%) charge, resulting in the minimum battery size of 197 (Wh) for first order, and 128.1 (Wh). For these calculations the efficiency of the converter connected to the battery is assumed to be 1.

$$E_{Battery} = \left(\frac{100\left|E_{peak}\right|}{100-45} \right)(2-\eta_{conv}) \tag{4.5}$$

For the gradient method a different initial state of charge of 38 (%) assumed will be assumed, due to the presence of a charging and discharging periods in Fig. 32. The calculated battery size needed for the gradient method is 320.2 (Wh).

The instantaneous power that needs to be provided for smoothing has to also be accounted for displayed in Fig. 36, which for the first order, second order, and gradient methods are as follows 728.8 (W), 765.7 (W), and 798.3 (W). It should be noted that the peaks of battery power during the other two day were lower than the ones in Fig. 36.

To summarize the battery sizes and peak powers per unit of the maximum rated power for 960 (W) for the PV panels required by the smoothing schemes are:

- LPF 1st Order $E_{Battery} = 0.2052$ and $P_{peakBattery} = 0.7592$
- LPF 2nd Order $E_{Battery} = 0.1334$ and $P_{peakBattery} = 0.7976$
- Gradient Method $E_{Battery} = 0.3335$ and $P_{peakBattery} = 0.8316$

If the retuning of the filter is done to meet the ramp rate limit for all three cases, as subjected both in the first and second order section, then the battery size will actually be a bit larger:

- LPF 1st Order $E_{Battery} = 0.2402$ and $P_{peakBattery} = 0.7609$
- LPF 2nd Order $E_{Battery} = 0.1573$ and $P_{peakBattery} = 0.7984$

From all the data so far, puts the second order low pass filter as the best smoothing method, it requires the smallest amount of battery, returns the battery to almost it initial level of charge, reduces the peak power the battery needs to provide in comparison with the gradient method. The implementation of the approach is quite straight forward. Drawbacks include the use of the battery during the clear sky days, and the tuning. The first order filter is inferior in every way to the second order, with the peak power needed. This suggests that maybe a higher order filter may additionally reduce the size of the battery needed. Finally, the gradient method can be viable depending on the profile of the weather where the PV system is locate, due to its ability to not use the battery during low variations in irradiance. However, it needs a larger battery capacity than the other schemes, thus it will be more expensive and more difficult to implement.

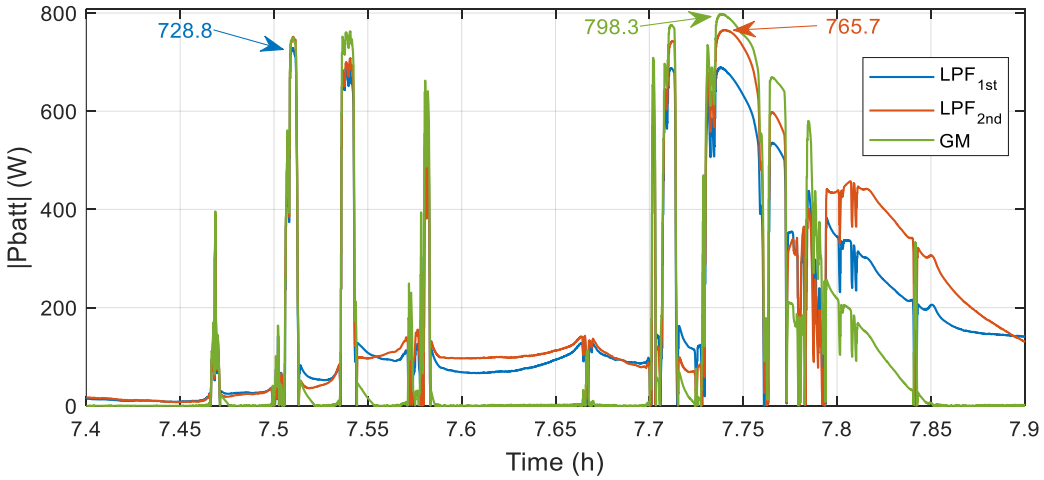

Fig. 36 Battery power used by the smoothing methods during high irradiance variation day

Chapter 5 Evaluation of Smoothing Methods – Experimental

The experimental setup consist of a Regatron PV simulator with maximum voltage of 1000 (V) and maximum current of 40 (A). After it we have a simple boost converter with nominal power of 1 (kW) and a maximum output voltage of 1000 (V). Additionally two inverters are present in the system, connected to a single phase power, and one of them acts as a battery emulator using the battery mode present in the control. The boost converter used a maximum power tracking scheme to provide the maximum active power possible. All the converters are controlled by the dSpace module, and the interface though which the system is controlled and the data is recorded is the Control Desk software. The complete setup can be seen in Fig. 37. It should additionally be mentioned that BP Solar MSX120 solar panels, eight in series, are simulated with the Regatron, and a general model of the Lithium-ion battery presented in chapter 3 is used. It has to be mentioned that the sampling frequency used in 8 (kHz).

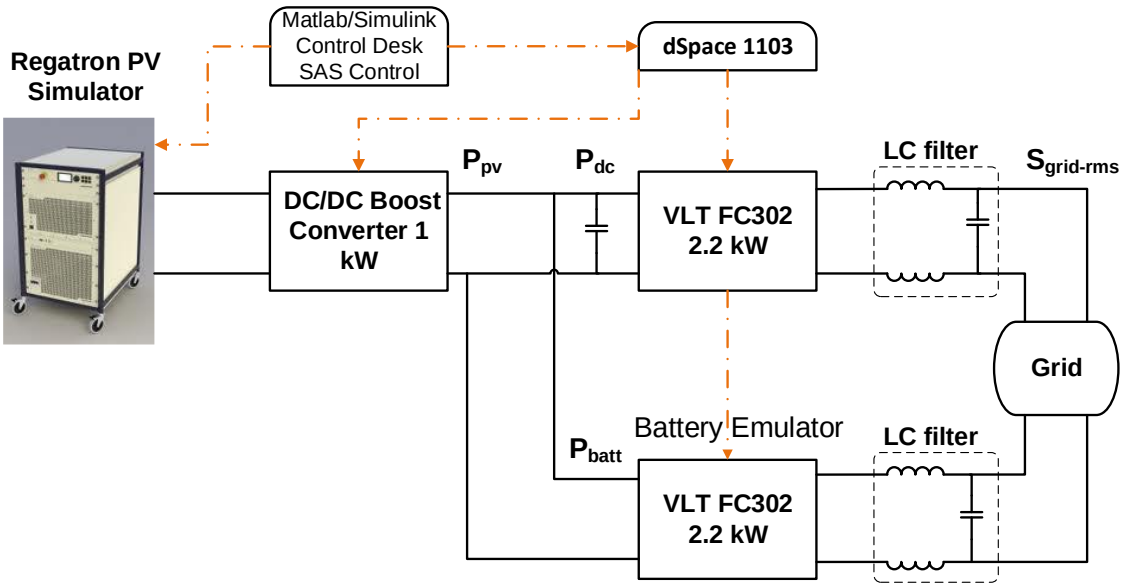

Fig. 37 Structure of experimental setup for power smoothing

To program an irradiance profile in the PV simulator requires a substantial time, since each ramp and the flat section has to be written in the code independently, which is time consuming, Thus a simplified profile is implemented to test the smoothing methods, which starts with a period of 180 (s) with an initial value of irradiance in 108 (W/m^2), because we want the maximum power point tracking to reach the maximum power. When this is done we can engage the smoothing method we want to test, also there is time to reset the gradient methods delays, so the method starts from the same point when the upward ramp begins. From 180 (s) to 240 (s) there is a 200 (W/m^2) change in irradiance, then a 150 (s) constant section follows to allow for the methods to settle.

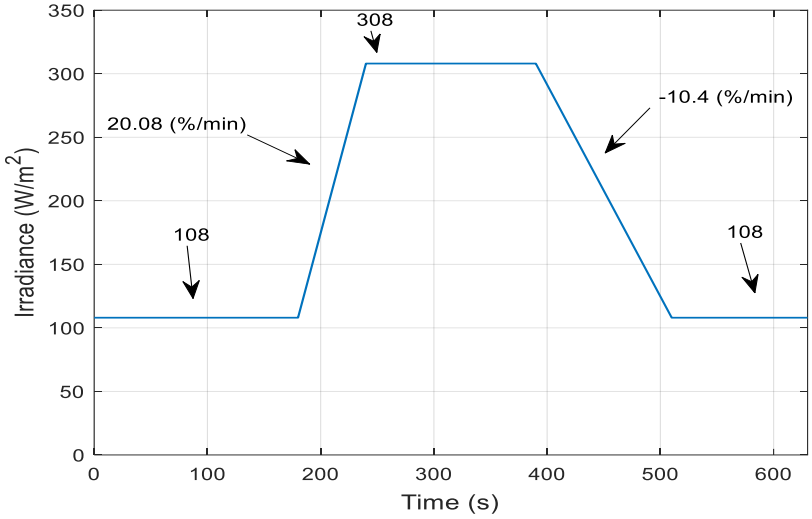

Fig. 38 Experimental irradiance profile

After that a change back to 108 (W/m^2) happens in the next 120 (s), and the final section with a constant value of 108 (W/m^2) lasts for another 120 (s), to allow for the approaches to settle, this irradiance profile can be seen in Fig. 38.

In Fig. 37 the points at which the different powers, i.e. PV power, battery power, are measured is shown. However P_{dc} is the exception since it is estimated from the sum of the measured P_{pv} and P_{batt}, since a measurement was not available.

A. First Order Low Pass Filter Method

For the first order filter a time constant of $T_f = 420\,(s)$ is used for both the experimental and simulation data in Fig. 39 where it can be observed that it mirrors closely the results achieved by the simulation. Differences can be noted in the reduced value of P_{pv} due to losses in the boost converter. It also should be mentioned there was a substantial amount of noise in the measured P_{pv}, due to the switching, which can be seen in Fig. 40. To reduce the noise and extract a more accurate value of the PV power, a first order low pass filter with a time constant of 0.5 (s) was used, its effect can be seen again in Fig. 40. The filter was placed before the smoothing block, P_{batt} also has to be filtered because of excessive noise, with the same filter parameters used for P_{pv}.

Looking at Fig. 39 we can see that the filter is too aggressive for the irradiance profile provided, leading to overcompensation of the ramp rate. Better result can be produced by reducing the time constant for the filter, which will lead to a higher ramp rate, less battery power used, and faster settling time.

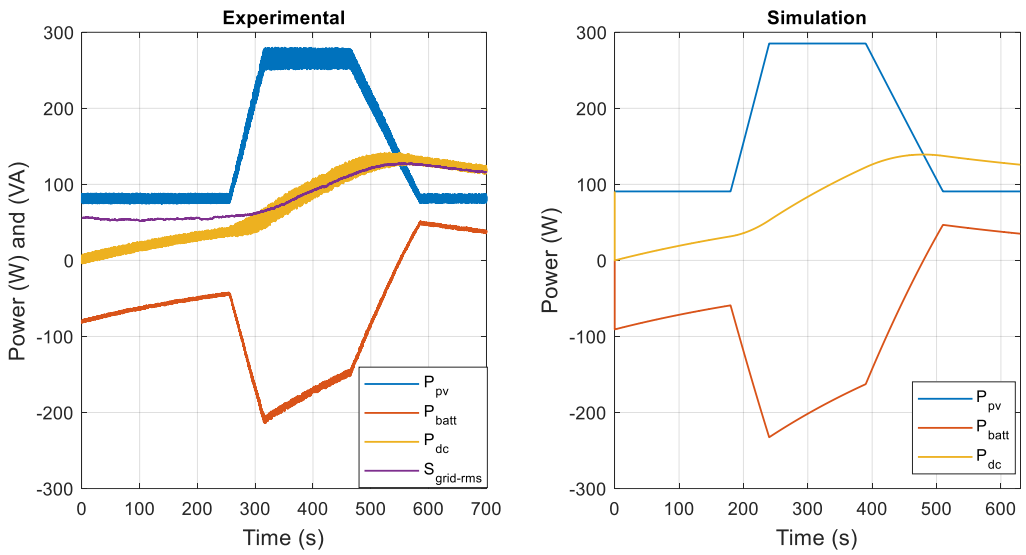

Fig. 39 Comparison between experimental and simulation data for first order LFP

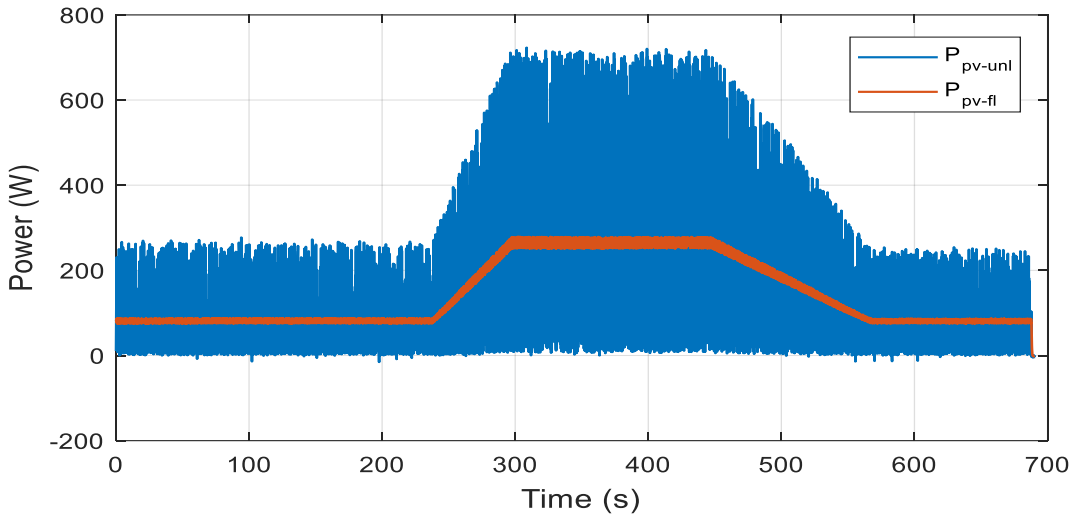

Fig. 40 Problem with the accurate accusation of PV power

B. Gradient Method

For the gradient method the noise present in the measurements leads to the incorrect calculation of derivative, and the approach was producing such a battery power reference, the P_{dc} had a very small slope. To correct for this problem, a noise was added to P_{pv} in the simulation model using a random number generator, to recreate the problem, and to test possible solutions. First a down sampling of P_{pv} and P_{batt} was tried in simulation and did not lead to significant improvements , then a first order low pass filter was used to reduce the noise. The gradient approach showed some improvement and was tested experimentally, the result is displayed in Fig. 41, where we can see that to make the method work as close to the ideal case as possible, quite an aggressive filter had to be used.

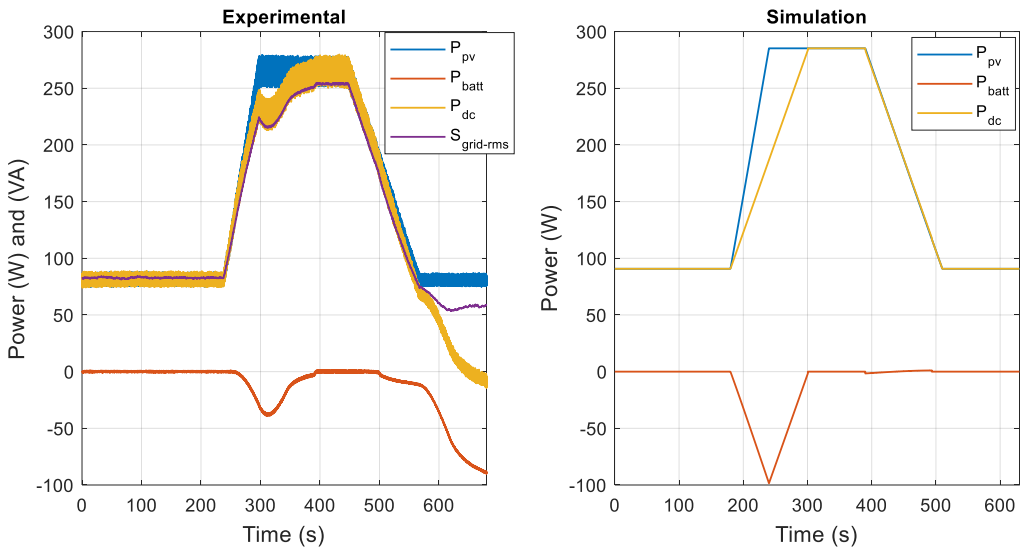

Fig. 41 Comparison between experimental and simulation data for gradient method

This lead to a delay in the filtered signal, which causes the gradient method to not limit the ramp rate of P_{pv} sufficiently

It must be noted that in Fig. 41 for the simulation plot the ideal case is used, where there is no noise in the measured signals. If we look at Fig. 42, where a random variation within the range of ±5 (W) is added to P_{pv}, we can see that without the filter almost all the energy is charged into the batter during the trapezoidal step. If a low pass filter is added the smoothing now becomes too little, as both the experimental data in Fig. 41 and the simulation data in Fig. 42, right plot, show. Even with a small noise of ±1 (W) the problem persisted, so it can be said that the numerical calculation of derivative is very sensitive to noise.

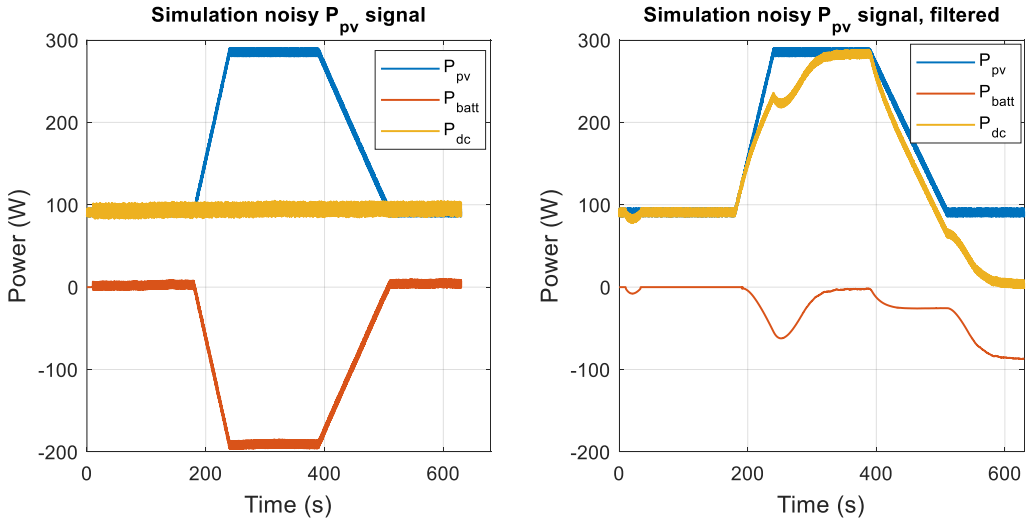

Fig. 42 Simulation of effect of unfiltered and filtered reference signal for gradient method

A possible solution to the problem is to measure the PV power before the boost converter, where the variation in power are smaller, and filter them if needed.

However this doesn't account for the efficiency of the boost converter, which will lead to a higher battery reference being generated by the gradient method, resulting in a less steep ramp rate than the one we desire.

C. Second Order Low Pass Filter Method

For the implementation of the second order filter a dampening ratio $\zeta = 0.707$ and a natural frequency of $w_n = 1/185(rad/s)$ is used. The same first order low pass filter is employed to suppress the noise, as was the case for the first order smoothing method, previously. If we look at Fig. 43 there is quite a good match, between the experimental and simulation results. Here again the filter is too aggressive in its smoothing, as was the case for the first order LPF. If both filter approaches are retuned with the irradiance profile on Fig. 38 in mind, better results can be achieved. One thing that can be mention here, when contrasting Fig. 39 and Fig. 43, is noted that the second order filter reaches a higher peak value, which confirm that, even though both filters are tuned using the same process, the second order filter allows for higher variation in the slopes below the ramp rate limit.

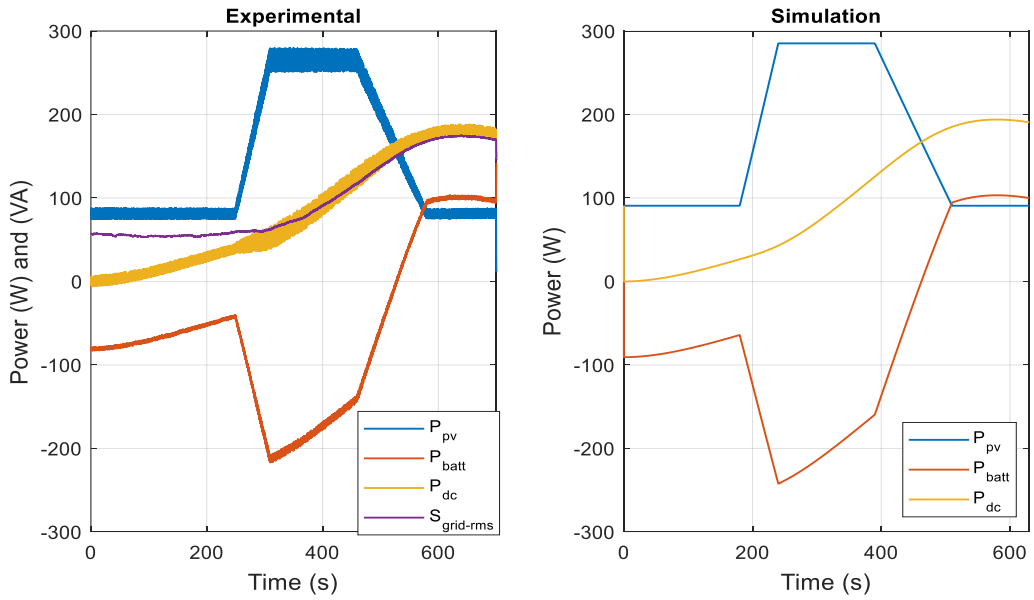

Fig. 43 Comparison between experimental and simulation data for second order LFP

Conclusions and future work

Both filter approaches for smoothing the power fluctuations, due to cloud movement, showed a good performance during the simulation and experimental tests. The second order filter proved to be the standout, when considering battery size, battery utilization, and using it will make the photovoltaic system expensive, compared with the other approaches.

The first order filter is the second best smoothing approach, when considering the initial investment for a PV system. It needs the second largest battery, and during the clear sky day, i.e. little variation in irradiance, uses the most energy.

Both filter approaches were easy to implement in practice, and can work with noisy signals, leading to them being quite robust.

The second order filter provides less smoothing to the ramp rates below the limit, than the first order filter, when they are tuned using the same criteria. This results in a smaller battery capacity needed for the second order LFP, to provide the desired smoothing.

Disadvantages associated with the low pass filters, are that they use the battery during a clear sky day, and lack of universal tuning procedure to derive the proper parameters, i.e. natural frequencies for different ramp rates. This can be investigated further in the future, since filters will probably be used for power smoothing applications in the future .

The gradient method seemed quite promising, using a dead zone function and a switch function, which did reduce battery usage, just not in a useful, way at least for the days when power smoothing is needed. The battery is not used at all during a clear sky day, however the battery capacity needed for the days with high irradiance, makes this the most expensive approach for power smoothing.

The gradient method leads to a low SOC of the battery, at the end of the day, for the high variation in irradiance days, and also needs the highest peak power, that either the battery needs to absorb or supply. Additionally, it is extremely sensitive to noise, which results in it being unreliable in a practical implementation.

A potential candidate for future investigation is a higher order low pass filter, which may further reduce the battery size needed for power smoothing. As happened with the second order filter, which improved upon the first order LPF in most areas, with the exception of the peak power required.

References

[1] A. Woyte, V. Van Thong, R. Belmans, and J. Nijs, "Voltage fluctuations on distribution level introduced by photovoltaic systems," *IEEE Trans. Energy Convers.*, vol. 21, no. 1, pp. 202–209, 2006.

[2] M. Rekinger, F. Thies, G. Masson, and S. Orlandi, "Global market outlook for solar power 2015–2019," 2015.

[3] D. K. Energinet, "Technical regulation 3.2. 2 for PV power plants with a power output above 11 kW," 2015.

[4] A. Sangwongwanich, Y. Yang, and F. Blaabjerg, "A Cost-Effective Power Ramp-Rate Control Strategy for Single-Phase Two-Stage Grid-Connected Photovoltaic Systems," in *Proceedings of the 8th Annual Ieee Energy Conversion Congress and Exposition, Ecce 2016*, 2016.

[5] N. Kakimoto, H. Satoh, S. Takayama, and K. Nakamura, "Ramp-rate control of photovoltaic generator with electric double-layer capacitor," *IEEE Trans. Energy Convers.*, vol. 24, no. 2, pp. 465–473, 2009.

[6] S. G. Tesfahunegn, Ø. Ulleberg, P. J. S. Vie, and T. M. Undeland, "PV Fluctuation Balancing Using Hydrogen Storage – a Smoothing Method for Integration of PV Generation into the Utility Grid," *Energy Procedia*, vol. 12, pp. 1015–1022, 2011.

[7] T. D. Hund, S. Gonzalez, and K. Barrett, "Grid-tied PV system energy smoothing," in *Conference Record of the IEEE Photovoltaic Specialists Conference*, 2010, pp. 2762–2766.

[8] M. J. E. Alam, K. M. Muttaqi, and D. Sutanto, "A Novel Approach for Ramp-Rate Control of Solar PV Using Energy Storage to Mitigate Output Fluctuations Caused by Cloud Passing," *IEEE Trans. Energy Convers.*, vol. 29, no. 2, pp. 507–518, 2014.

[9] B. Diouf and R. Pode, "Potential of lithium-ion batteries in renewable energy," *Renewable Energy*, vol. 76. pp. 375–380, 2015.

[10] J. Li and M. A. Danzer, "Optimal charge control strategies for stationary photovoltaic battery systems," *J. Power Sources*, vol. 258, pp. 365–373, 2014.

[11] Y. Riffonneau, S. Bacha, F. Barruel, and S. Ploix, "Optimal Power Flow Management for Grid Connected PV Systems With Batteries," *IEEE Trans. Sustain. Energy*, vol. 2, no. 3, pp. 309–320, 2011.

[12] M. Datta, T. Senjyu, A. Yona, T. Funabashi, and C. H. Kim, "Photovoltaic output power fluctuations smoothing methods for single and multiple PV generators," *Curr. Appl. Phys.*, vol. 10, no. 2 SUPPL., 2010.

[13] H. Liu, J. Peng, Q. Zang, and K. Yang, "Control Strategy of Energy Storage for Smoothing Photovoltaic Power Fluctuations," *IFAC-PapersOnLine*, vol. 48, no. 28, pp. 162–165, 2015.

[14] A. Ellis, D. Schoenwald, J. Hawkins, S. Willard, and B. Arellano, "PV output smoothing with energy storage," in *Conference Record of the IEEE Photovoltaic Specialists*

Conference, 2012, pp. 1523–1528.

[15] R. Van Haaren, M. Morjaria, and V. Fthenakis, "Utility scale PV plant variability and energy storage for ramp rate control," in *Conference Record of the IEEE Photovoltaic Specialists Conference*, 2013, pp. 973–979.

[16] T. R. E. am Mittelspannungsnetz, "Richtlinie für Anschluss und Parallelbetrieb von Erzeugungsanlagen am Mittelspannungsnetz," *BDEW, Ausgabe Juni*, 2008.

[17] B.-I. Crăciun, T. Kerekes, D. Séra, R. Teodorescu, and U. D. Annakkage, "Power ramp limitation capabilities of large PV power plants with active power reserves," *IEEE Trans. Sustain. Energy*, vol. 8, no. 2, pp. 573–581, 2017.

[18] V. Gevorgian and S. Booth, "Review of prepa technical requirements for interconnecting wind and solar generation," *Natl. Renew. Energy Lab. Natl. Renew. Energy Lab. Golden, CO, Tech. Rep. No. NREL/TP-5D00-57089*, 2013.

[19] D. L. King, W. E. Boyson, and J. A. Kratochvil, "Photovoltaic array performance model," *Sandia Rep. No. 2004-3535*, vol. 8, pp. 1–19, 2004.

[20] O. Tremblay and L. A. Dessaint, "Experimental validation of a battery dynamic model for EV applications," *World Electr. Veh. J.*, vol. 3, no. 1, 2009.

[21] A. Makibar, L. Narvarte, and E. Lorenzo, "On the relation between battery size and PV power ramp rate limitation," *Sol. Energy*, vol. 142, pp. 182–193, 2017.